AAC Accepted Manuscript Posted Online 23 March 2020
Antimicrob. Agents Chemother. doi:10.1128/AAC.00123-20
Copyright © 2020 American Society for Microbiology. All Rights Reserved.

Accepted Manuscript Posted Online
Antimicrobial Agents and Chemotherapy
AAC
Antimicrobial Agents and Chemotherapy

Downloaded from http://aac.asm.org/ on April 2, 2020 at GSF/ZENTRALBIBLIOTHEK

Structure and molecular recognition mechanism of IMP-13 metallo-β-lactamase

Charlotte A. Softley[a,b,1], Krzysztof M. Zak[b,1], Mark J. Bostock[a,b,1], Roberto Fino[a,b], Richard Xu Zhou[a,b], Marta Kolonko[b,c], Ramona Mejdi-Nitiu[d], Hannelore Meyer[d], Michael Sattler[a,b,*], Grzegorz M. Popowicz[a,b,*]

[a] Biomolecular NMR and Center for Integrated Protein Science Munich at Department Chemie, Technical University of Munich, Lichtenbergstraße 4, 85747, Garching, Germany.

[b] Institute of Structural Biology, Helmholtz Zentrum München, Ingolstädter Landstraße 1, 85764 Neuherberg, Germany.

[c] Department of Biochemistry, Faculty of Chemistry, Wroclaw University of Science and Technology, Wybrzeze Wyspianskiego 27, 50-370, Wroclaw, Poland

[d] Institute for Medical Microbiology, Immunology and Hygiene, Technical University of Munich, Trogerstraße 30, 81675 München, Germany

[1] **These authors contributed equally to this work. The order of these authors was determined by the order in which they joined the project.**

* corresponding author emails:

grzegorz.popowicz@helmholtz-muenchen.de; michael.sattler@helmholtz-muenchen.de;

Abstract

Multi-drug resistance among Gram-negative bacteria is a major global public health threat. Metallo-β-lactamases (MBLs) target the most widely-used antibiotic class, the β-lactams, including the most recent-generation carbapenems. Interspecies spread renders these enzymes a serious clinical threat

Accepted Manuscript Posted Online

and there are no clinically-available inhibitors. We present crystal structures of IMP-13, a structurally-uncharacterized MBL from Gram-negative *Pseudomonas aerugionasa* found in clinical outbreaks globally, and characterize the binding using solution NMR-spectroscopy and molecular-dynamics simulations. Crystal structures of apo IMP-13 and bound to four clinically-relevant carbapenem antibiotics (doripenem, ertapenem, imipenem and meropenem) are presented. Active site plasticity and the active-site loop, where a tryptophan residue stabilizes the antibiotic core scaffold, are essential to the substrate-binding mechanism. The conserved carbapenem scaffold plays the most significant role in IMP-13 binding, explaining the broad substrate specificity. The observed plasticity and substrate-locking mechanism provide opportunities for rational drug design of novel metallo-β-lactamase inhibitors, essential in the fight against antibiotic resistance.

Keywords

IMP-13; metallo-β-lactamase; imipenemase; antibiotic resistance; solution NMR; X-ray crystallography; molecular dynamics; metalloenzyme; protein dynamics; β-lactam antibiotic

Introduction

Multidrug-resistant bacteria pose a major challenge to human health, with resistance mechanisms to all known classes of antibiotics now identified. While much pharmaceutical research has focused on drugs to treat Gram-positive infections, multidrug resistance amongst Gram-negative pathogens remains a significant clinical challenge (1-3). β-lactam antibiotics are used in treatment of both Gram-negative and Gram-positive bacterial infections and are the most commonly prescribed antibiotics (4, 5). β-lactam antibiotics act as inhibitors of cell wall biosynthesis, causing subsequent bacterial cell death (6). The success of the first β-lactam antibiotic, penicillin, discovered in 1928 by

Antimicrobial Agents and Chemotherapy
AAC
Antimicrobial Agents and Chemotherapy
Downloaded from http://aac.asm.org/ on April 2, 2020 at GSF/ZENTRALBIBLIOTHEK

Accepted Manuscript Posted Online

Antimicrobial Agents and Chemotherapy

AAC

Antimicrobial Agents and Chemotherapy

Downloaded from http://aac.asm.org/ on April 2, 2020 at GSF/ZENTRALBIBLIOTHEK

Alexander Fleming (7) and used clinically since 1943 (8), led to multiple developments of the β-lactam scaffold providing new and more effective antibacterial compounds.

As a result of the widespread use of β-lactam antibiotics, resistance mechanisms against them have emerged (3). Resistance mechanisms can be divided into mutated penicillin binding proteins (PBPs), which prevent binding of β-lactams to their target protein; reduction of antibiotic concentration in the cell due to increased efflux (expression of efflux pumps) or decreased uptake (altered expression of outer membrane proteins) and, most commonly and significantly, production of β-lactamase enzymes (9). β-lactamases hydrolyze the β-lactam ring, which distinguishes this class of antibiotics and is key to its binding mechanism, thus preventing interaction of the antibiotic with its target (10). As a response to the emergence of enzyme-mediated resistances as early as the 1940s (11), cephalosporin and carbapenem-type β-lactam antibiotics were discovered, isolated and developed (12-14). Carbapenems are formed of a core scaffold, consisting of a β-lactam ring fused to a pyrroline ring that is decorated with an exocyclic sulfur that links to the tail region of the molecule (Fig. SI1).

However, β-lactamases that are capable of inactivating the most recent generation carbapenems, often used as a last-resort for effective treatment against multidrug-resistant bacteria, have now evolved (15) and spread rapidly (16). As such, carbapenem resistance is a hallmark of all three of the World Health Organisation's highest priority pathogens (17).

On a structural basis, four main classes of β-lactamases can be defined - three classes of serine β-lactamases, distinguishable by their amino acid sequence and inhibitor susceptibility (Ambler class A, C and D) and one class of metallo-β-lactamases (B), requiring divalent zinc ions for their β-lactamase activity (18). MBLs have been shown to hydrolyze all bicyclic β-lactams including the carbapenems (19). The existence of MBL genes on integron structures and plasmids, often co-expressed with other antibiotic resistance genes, renders MBLs a serious clinical challenge, due to the possibility of horizontal gene transfer (20, 21). Inhibitors of serine β-lactamases, e.g. clavulanic acid (22) and

Accepted Manuscript Posted Online

avibactam (23), are available and used clinically in combination with antibiotics (24). However, resistance to this treatment is already being seen in the clinic (25) and to date there are no clinically available inhibitors of the class B MBLs, making MBLs a significant threat.

MBLs can be divided into three subclasses (B1, B2 and B3), based on sequence and structural similarities and the number of coordinated zinc ions, with the B1 class representing the most significant clinically (26). Among the major B1 class enzymes are the imipenemases (IMP), Verona integron-encoded MBLs (VIM) and the New Delhi MBLs (NDMs), which can hydrolyze the most recent cephalosporins and carbapenems (20, 27, 28).

IMP-type MBLs were first identified in Japan, and the class now consists of at least 53 members (29, 30) identified in more than 26 species of Gram-negative bacteria from around the world (31). IMP-encoding genes have been shown to occur as resistance cassettes along with other resistance genes, including those of serine β-lactamases (32), and aminoglycoside (33) and streptomycin (34) resistances. IMPs can be divided into six subgroups based on phylogeny and sequence similarity. IMP-13, a member of subgroup 2 sharing 92.3% amino acid sequence similarity with IMP-2 and 82.5% with IMP-1 (Fig. SI2 (35)), was first identified in the Gram-negative pathogen *Pseudomonas aeruginosa* from clinical samples in Italy (21) and is a common cause of carbapenem resistance, often involved in large outbreaks (36). IMP-13 has been detected in a number of other countries in Europe as well as South America (21, 36-38). While IMP-13 is most commonly associated with *Pseudomonas aeruginosa* infections, it has also been identified in other human pathogens including *Salmonella enterica*, members of the *Enterobacteriaceae*, including *Klebsiella* and *Enterobacter* spp. (38, 39), as well as non-human pathogens in the environment e.g. *Pseudomonas monteilii*, related to the soil microbe *P. putida* (40). These studies indicate that IMP-13 is present in a variety of significant human pathogens, as well as in other non-human pathogens which can act as environmental reservoirs of antibiotic resistance.

Antimicrobial Agents and Chemotherapy
AAC
Antimicrobial Agents and Chemotherapy
Downloaded from http://aac.asm.org/ on April 2, 2020 at GSF/ZENTRALBIBLIOTHEK

Accepted Manuscript Posted Online

Antimicrobial Agents and Chemotherapy

AAC

Antimicrobial Agents and Chemotherapy

Downloaded from http://aac.asm.org/ on April 2, 2020 at GSF/ZENTRALBIBLIOTHEK

95 Recombinant IMP-13 protein has been overexpressed, purified and characterized biochemically (41),
96 but no structural information concerning IMP-13 has yet been reported. Crystal structures of MBLs,
97 such as NDM-1 and IMP-1 show a conserved αβ/βα fold, with an active site at the interface of the
98 two αβ units involving one or two zinc ions (42, 43). Although the overall folds are expected to be
99 very similar, divergence between the various structures makes these challenging targets for drug
100 development. Currently relatively few crystal structures are available for other members of the IMP
101 class, with no structural information on the antibiotic binding mode. Thus, high-resolution structural
102 information is essential to broaden overall knowledge of MBLs and their antibiotic binding modes
103 and enable the design of novel β-lactamase inhibitors to fight antibiotic resistance. Plasticity of the
104 active site is also seen to play a role in other MBL classes (44, 45) so analysing a wide range of
105 antibiotic binding modes will help to determine the key factors in this.

106 Herein, we report two distinct apo IMP-13 structures and the structures of four complexes with
107 clinically-relevant carabapenem antibiotics bound in their hydrolyzed form (doripenem, ertapenem,
108 imipenem and meropenem). We also present backbone NMR assignments and NMR relaxation
109 measurements for IMP-13 in the apo and ertapenem-bound forms, and molecular dynamics
110 simulations for the apo and carbapenem-bound states. The structural information and dynamics
111 presented here reveals important information about the mechanism of antibiotic binding, as well as
112 a significant role for the active site covering loop (L1), indicating that the plasticity of the active-site
113 region is important for the broad substrate-recognition spectrum of these enzymes. The structural
114 information presented here provides important information to further aid in the development of
115 novel MBL inhibitors, essential to combat this significant bacterial threat.

116

Accepted Manuscript Posted Online

Antimicrobial Agents and Chemotherapy

AAC

Antimicrobial Agents and Chemotherapy

Downloaded from http://aac.asm.org/ on April 2, 2020 at GSF/ZENTRALBIBLIOTHEK

Results

Structure of the apo-form of IMP-13

Two apo-form crystal structures of IMP-13, showing the L1 active-site loop (Fig. 1, SI3, SI4) in open and closed conformations, were solved to 1.9 and 2.2 Å resolution respectively (PDB: 6R78 and 6R79). We define the "open" conformation as the loop pointing away from the protein towards the solvent and the "closed" as the loop positioned over the active site and pointing towards its rim. The distance between Cα of the Trp28 for open and closed conformation is 8.8 Å . The overall protein architecture of the IMP-13 apo structure is consistent with the previously-published metallo-β-lactamase fold (43), consisting of a global αβ/βα topology, with a shallow active-site cleft at the border of the two β-sheets. In the apo structure presenting a closed L1 loop conformation (apo_{closed} conformation, PDB: 6R78), the two divalent zinc ions are found a distance of 3.5 Å apart: one (Zn1) coordinates His77, His79 and His139 residues and a bridging water molecule in a tetrahedral geometry, while the other (Zn2) coordinates Asp81, Cys158 and His197 and the bridging water (Fig. 1B). The bridging water was proposed by Page and colleagues to be in the form of a hydroxide ion for activation of the β-lactam ring for hydrolysis (46, 47) and is seen to be around 3.3 Å from each of the oxygens of the Asp81 sidechain, indicating that the hydroxide ion would be oriented by these residues as seen in IMP-1 (48). In the apo_{open} structure (PDB: 6R79), the conformation is determined by interlocking with another loop, while in the closed conformation these interactions are missing. The B-factor values of the loop residues are in both cases approximately 20 $Å^3$ higher than the rest of the protein molecule, indicating high flexibility of this region.

Structure of carbapenem-bound IMP-13

Crystal structures of IMP-13 bound to hydrolyzed doripenem (2.8 Å, PDB: 6S0H), ertapenem (2.2 Å, PDB: 6RZS), imipenem (1.9 Å, PDB: 6RZR) and meropenem (2.3 Å, PDB: 6R73) were solved by molecular replacement, with IMP-13 antibiotic complex crystals prepared by co-crystallization. Both the tautomers with sp2 and sp3 carbons at the C4 position of the carbapenems (46) (all without a

Accepted Manuscript Posted Online

Antimicrobial Agents and Chemotherapy

AAC

Antimicrobial Agents and Chemotherapy

Downloaded from http://aac.asm.org/ on April 2, 2020 at GSF/ZENTRALBIBLIOTHEK

142 hydrogen on N6) were modelled into the ligand electron density and refined separately. As the
143 resolution of the collected data is moderate and does not allow clear differentiation between the
144 two tautomers, and with an understanding that the crystal structure may be a weighted average of
145 the two forms, the tautomer with the lowest B factor, the sp2 form, was deemed to be the most
146 representative in all cases (Fig. 2), as C4 attached to the S is not visibly tetrahedral. From this, with
147 respect to the mechanisms shown in Lisa et al. (49) and Feng et al. (46) , we believe that the primary
148 state visible is that of the intermediate EI_2. According to Lisa et al., this would then become the Δ1
149 form after addition of the hydrogen via the sulphur-bound carbon atom and so could be a weighted
150 average of these two states. In all the structures, the tail moiety of the carbapenem adopts different
151 positions when bound to chain A or B of the crystal structure. Such an arrangement can be explained
152 by the location of the tail, which experiences crystal packing contacts in one chain and solvent-
153 exposure in the other chain, resulting for the latter in high flexibility and rotational freedom,
154 demonstrated by increased B-factor values compared to the core atoms of the carbapenem scaffold.
155 Further description focuses on chain B of the doripenem, ertapenem and imipenem-bound
156 structures and chain A of meropenem, where crystal packing is not seen to affect ligand placement.

157 A comparison of the carbapenem-bound complex structures with apo_{closed} elicits very few distinct
158 differences with the L1 loop seen packed over the antibiotic binding pocket (Fig. 1A, C, D). The RMSD
159 of the backbone Cα atoms (for 216 out of 217 residues), including the L1 loop, varies from 0.27 to
160 0.47 Å, showing a high level of structural similarity between the structures, with only a few
161 differences in the flexible loop regions. With the apo_{open} structure on the other hand, the loop can be
162 seen pointing away from the active site, leaving it the active site accessible to the substrate (Fig. 1A).
163 The tunnel formation as seen in the closed form is completely absent due to different positioning of
164 both backbone and side-chain atoms. In the complex structures, the largest active-site-facing
165 changes seen in the L1 loop occur between residues Val25 and Val31, with these two residues
166 moving towards the carbapenems to form hydrophobic interactions (movements are in the range of
167 5 Å and 1 Å for the Val25 and Val31, respectively). The residues located in the middle of the L1 loop,

Accepted Manuscript Posted Online

Val25 and Trp28, show more significant changes, moving approximately 9–10 Å in order to cover the substrate during catalysis, thereby closing the tunnel-like structure above the active site of the enzyme and acting as a gatekeeper between the ligand and the solvent. Further conformational differences between apo and carbapenem-bound structures include movement of Asn167 closer to the active site in order to facilitate the hydrogen bonding with the substrate (the rest of the L3 loop does not alter its conformation significantly). Strands B7 and B8 are also altered between the open and closed protein conformations, with Tyr123 and Trp124 showing the most pronounced changes.

Compared to the apo structures the zinc ions in carbapenem-bound IMP-13 are located slightly further apart with the distance for the different antibiotics ranging from 3.8 Å (doripenem complex) to 4.22 Å (ertapenem complex) compared to 3.5 Å for the apo state, presumably to maximise interactions with the ligand. The zinc-protein coordination remains unchanged (Fig. SI5): Zn1 still coordinates the three histidines (His77, 79 and 139), whilst Zn2 coordinates Asp81, Cys158 and His197, but the bridging water is no longer observed due to the presence of the enzyme's substrate.

Conserved binding mode of the carbapenem scaffold to IMP-13

Binding of the carbapenem scaffold (Fig. 2, SI1) is similar for the four antibiotics investigated, with contacts created with the surrounding residues via a network of hydrogen bonds and hydrophobic and electrostatic interactions. In the carbapenem complexes, two loops, L1 and L3 (Fig. 2, SI3, SI4), interact with the hydrolyzed substrates (Fig. SI6). Both zinc ions show an interaction with N6 on the pyrroline ring, with Zn2 having a closer interaction (SI Table 1, Fig. SI5). In addition, there are interactions with carboxylic acid moieties O9, O26 and O27. In all cases, Zn1 coordinates O9, while Zn2 coordinates O26 and O27. Lys161 acts as a counterion to the carboxylate of the carbapenems (O8, O9). Hydrogen bonding is observed between the carbapenems' hydroxyl groups (O24) and the Asp81 backbone nitrogen. Interactions are also observed to the Asp81 sidechain, and between the sidechain of Asn167 and the carbapenems' hydroxyls (O26, O27).

Antimicrobial Agents and Chemotherapy
AAC
Antimicrobial Agents and Chemotherapy
Downloaded from http://aac.asm.org/ on April 2, 2020 at GSF/ZENTRALBIBLIOTHEK

Accepted Manuscript Posted Online

Antimicrobial Agents and Chemotherapy

AAC

Antimicrobial Agents and Chemotherapy

Downloaded from http://aac.asm.org/ on April 2, 2020 at GSF/ZENTRALBIBLIOTHEK

193 L1, the extended β loop that is conserved in β-lactamases, encompasses the active site, forming a
194 tunnel-like structure of a hydrophobic nature (Fig. 1C, 1D); the amino acid composition of L1 results
195 in hydrophobicity index of 0.84 (50), in comparison to the overall protein at -0.32. This largely
196 hydrophobic loop interacts with the β-lactam antibiotics, stabilizing their position during hydrolysis.
197 The tryptophan (Trp28) at the tip of this loop is a key residue that bridges the gap between the loop
198 backbone and the active site residues, forming a closed tunnel. In IMP-1, the equivalent tryptophan
199 is found to affect K_m: for imipenem, a W64A mutant leads to a five-fold increase in K_m (51). The
200 sulfur atom present in the linker region (S10) of all carbapenems creates strong π-sulfur interactions
201 with the aromatic ring of Trp28 (as well as interacting with the backbone of Asn167), thereby
202 contributing to the position of the core scaffold of all presented carbapenem substrates. Due to the
203 multiple tail conformations in imipenem, the orientation for the π-sulfur interaction in this case is
204 not always optimal, however the distance remains consistent. In addition, Trp28 shows interactions
205 with the pyrroline methyl group (C21), present in all the antibiotics studied other than imipenem.
206 These interactions lead to restricted motion in the side chain of Trp28, which further rigidifies the L1
207 loop (Fig. 3). The lack of this interaction in imipenem, could lead to a reduction in binding
208 interactions to the loop and may contribute to the observed reduction in affinity (increase in K_m) for
209 imipenem (SI Table 2). It is likely that there is a hydrophobic interaction between the ring itself and
210 the tryptophan in the absence of this methyl. Two other hydrophobic L1 residues, Val25 and Val31,
211 also form alkyl interactions with C21 where present.

212 **Binding modes of the antibiotic tails to IMP-13**

213 Analysis of the interactions between the carbapenem tail moieties and the surrounding residues and
214 solvent molecules shows a complex network of position-dependent contacts. Due to the presence of
215 more than one molecule in the unit cell, a representative molecule was chosen for discussion where
216 the crystal packing does not affect the antibiotic tail placement. Higher solvent accessibility of the
217 tails leads to less restrained positions, characterized by increased B factor values.

Accepted Manuscript Posted Online

Antimicrobial Agents and Chemotherapy

AAC

Antimicrobial Agents and Chemotherapy

Downloaded from http://aac.asm.org/ on April 2, 2020 at GSF/ZENTRALBIBLIOTHEK

The most solvent-exposed parts of the four antibiotics are very distinct, while in addition imipenem has no pyrrolidine ring in the antibiotic tail. The pyrrolidine ring of meropenem, doripenem and ertapenem is suitably located to form aromatic, π-alkyl interactions with His197 and is further stabilised by the hydrophobic environment created by Val25 and Val31. The terminal NMe_2 group of meropenem is stabilized by direct, as well as water-mediated interactions with the backbone of His163 and Gly164 and π-alkyl interactions with Trp28. The sulfonamide moiety of doripenem forms several hydrogen bonds: the nitrogen of the primary amine group interacts with Thr32 and the backbone of Val30, whilst the oxygen creates hydrogen bonds with backbone and sidechain atoms of Thr32. The terminal part of the imipenem tail was modelled in three different conformations (50%:25%:25% occupancy) highlighting the extreme flexibility of this moiety. Due to the different conformers, the interaction network is different in every modelled position - conformer A creates a hydrogen bond with the backbone carbonyl of Val30 and water-mediated hydrogen bonds with the backbone of Thr32. The most solvent-exposed conformation, conformer B, lacks interactions with surrounding residues, most likely interacting with a water network, while conformer C interacts with the wider water network. In each case, a water molecule replaces the amine group from the other two conformer positions.

NMR measurements show altered dynamics in presence and absence of antibiotic

As discussed above, the L1 loop adopts very different conformations in the two apo structures (apo_{closed} and apo_{open}). In apo_{closed}, the loop is folded over the active site, whilst in the apo_{open} structure, L1 is extended away from the protein, leaving the active site accessible. In complex with each of the hydrolyzed carbapenems, this loop forms a tightly locked, tunnel-like structure around the hydrolyzed antibiotic (Fig. 1D), with several hydrophobic interactions appearing to stabilize this state.

Accepted Manuscript Posted Online

Antimicrobial Agents and Chemotherapy

AAC

Antimicrobial Agents and Chemotherapy

Downloaded from http://aac.asm.org/ on April 2, 2020 at GSF/ZENTRALBIBLIOTHEK

242 To further understand the role of the L1 loop in antibiotic binding, NMR spectra were acquired for
243 IMP-13 in the apo state and bound to ertapenem. An overlay of $^{1}H,^{15}N$ HSQC spectra for the two
244 forms (Fig. SI7) shows substantial chemical shift changes on addition of ertapenem, necessitating
245 backbone assignment using triple resonance spectra in both forms. $^{1}H,^{15}N$ assignments were
246 achieved for 203 residues in the apo form (93%) and 195 residues in the ertapenem-bound form
247 (89%) from a total of 219 residues (excluding the 9 prolines) Assignments are shown in Fig. SI8 for
248 the apo state and Fig. SI9 for the ertapenem-bound state.

249 Chemical shift perturbations are shown in Fig. 4 and plotted on the ertapenem-bound structure
250 (PDB: 6RZS). The largest changes are colored in red on the structure and predominantly localize to
251 loops in the vicinity of the ertapenem-binding pocket. These changes are also marked with arrows
252 on the spectra shown in Fig. SI7. As expected, significant shifts are seen for residues in the L1 loop
253 (marked with red boxes on Fig. 4), in particular residues Glu24, Gly27, Trp28, Thr32 and Lys33 as well
254 as the side-chain NεHε of Trp28; the L3 loop (residues 163–166, especially residue Gly166), which
255 lies in the vicinity of the ertapenem tail and residue Asp81, which coordinates Zn2 as well as in the
256 linker between B11 and A5 (residues 197–201). Smaller changes are seen in the β-strands, B9, B10
257 and B11. These changes are consistent with the observations in the crystal structure (above).

258 Heteronuclear ^{1}H-^{15}N NOE (hetNOE) experiments were acquired to detect fast picosecond-
259 nanosecond (ps-ns) timescale motions (52, 53). Typically, structured regions of the protein show
260 hetNOE values > 0.8, while flexible loops and the N- and C-termini show lower values, < 0.8. Fig. 5
261 shows an overlay of the heteronuclear NOE values for the apo and ertapenem-bound forms. Both
262 states show similar values with an average hetNOE value, taken across backbone residues Asp6 to
263 Glu219, of 0.783 (standard deviation 0.078) for the apo form and 0.799 (standard deviation 0.096)
264 for the ertapenem-bound form. However, notably lower values are recorded in the L1 loop in the
265 apo state, with values of 0.51 and 0.46 for residues Asn26 and Gly29 respectively whereas in the
266 ertapenem-bound state, values do not drop below 0.6 in this region. Most significantly, Trp28 NεHε

Accepted Manuscript Posted Online

Antimicrobial Agents and Chemotherapy

AAC

Antimicrobial Agents and Chemotherapy

267 has a hetNOE of 0.3 in the apo form, which rises to 0.77 in the ertapenem-bound state, comparable
268 to backbone amides in structured regions of the protein, indicating a significant change in dynamic
269 properties. This suggests that in the apo form the L1 loop is undergoing fast-timescale motions,
270 while binding of antibiotic in the active site stabilizes the L1 loop. The restricted motion of Trp28
271 NεHε suggests that the antibiotic interacts with this residue reducing fast-timescale motions at this
272 position. The hetNOE data shows slightly more restriction in residues 165-168 in the presence of
273 ertapenem, but residue Gly164 is considerably more flexible in both the apo and ertapenem-bound
274 states. It was not possible to assign residues at the beginning of the L3 loop suggesting unfavourable
275 dynamics in this region.

276 **Molecular dynamics simulations show significant variations in L1 loop dynamics between complex**
277 **structures**

278 The distinct conformations observed in the two apo crystal structures and the NMR relaxation data
279 indicate that the L1 loop is likely to be flexible in solution. We therefore performed molecular
280 dynamics (MD) simulations to assess the movement and flexibility of this protein fragment on the
281 nanosecond time scale for the apo and carbapenem-bound structures (Fig. 3). During a total
282 simulation time of 50 ns for each system, all systems showed no significant large-scale fluctuations,
283 indicating that the solute systems were stable. In addition, the ligand RMSD values (SI Table 3)
284 suggest that the conformation of the hydrolyzed ligands remains stable during both the 50 ns and
285 100 ns simulation times. Torsion angles were also generally maintained throughout both the
286 simulation runs. Excluding the intrinsic flexibility of L1, the protein overall does not undergo
287 significant conformational changes aside from the active-site region.

288 However, the simulations reveal significant changes in L1 behaviour between the different
289 structures. Lower root-mean-square fluctuations (RMSFs) for heavy atoms of L1 residues in the
290 simulated doripenem, ertapenem and meropenem-bound complex structures when compared to
291 those of apo_{closed} indicate that L1 is more rigid in the closed conformation when these ligands are

Downloaded from http://aac.asm.org/ on April 2, 2020 at GSF/ZENTRALBIBLIOTHEK

Accepted Manuscript Posted Online

Antimicrobial Agents and Chemotherapy

AAC

Antimicrobial Agents and Chemotherapy

Downloaded from http://aac.asm.org/ on April 2, 2020 at GSF/ZENTRALBIBLIOTHEK

292 bound, while in the apo protein, L1 can move with a higher degree of freedom. This is shown by the
293 Cα RMSF being 1.4, 2.1 and 1.9 Å larger in the apo structure than in the doripenem-, ertapenem- and
294 meropenem-bound forms respectively (1.1, 1.4 and 0.8 for the replicas). However, while the
295 behaviour of L1 is comparable and shows the greatest restriction for the doripenem, ertapenem and
296 meropenem bound structures, it differs significantly for the imipenem complex, which is comparable
297 to the apo form (Fig. 3C,E). In the X-ray structures, interaction of bound ertapenem and meropenem
298 with the Trp28 sidechain occurs via the sulfur adjacent to the β-lactam ring and additionally via the
299 methyl group on the pyrroline ring. In contrast, imipenem lacks this additional methyl group, which
300 reduces the strength of the lipophilic interaction with the Trp28 side-chain, thus resulting in greater
301 loop flexibility. Furthermore, as shown by both shorter and longer overall simulation times for all the
302 complexes, the tail of imipenem shows high flexibility and occupies multiple rotamer positions, and
303 thus does not contribute further to the loop stability. Doripenem, however, does contain both a
304 sulfur-π and a methyl-π interaction, but the MD simulation shows a higher motility of the
305 sulfonamide tail of the hydrolyzed antibiotic (atoms N18, N19, O21, O22 and S28, Fig. 3A). This is in
306 agreement with the chemical character of this moiety which, due to a higher energy contribution to
307 desolvation, is more prone to interact with nearby solvent molecules, thus leading to a markedly
308 higher RMSF for the atoms in the antibiotic tail in comparison to ertapenem and meropenem
309 structures.

310

311 ## Discussion

312 We present apo and complex structures of IMP-13, bound to hydrolyzed carbapenems.
313 Imipenemases represent one of the major groups of class B1 metallo-β-lactamases found in Gram-
314 negative pathogens, which can hydrolyze all bicyclic β-lactam antibiotics. This includes carbapenems,
315 which are often reserved as the last resort for treatment in cases of multidrug resistance. There are
316 relatively few structures of imipenemase enzymes available, and no structures bound to

Accepted Manuscript Posted Online

carbapenems. Currently no inhibitors of metallo-β-lactamases are available in the clinic. Consequently, understanding the structural features of carbapenem interactions with a member of the imipenemase class is essential to developing new inhibitors to treat multidrug resistant pathogens.

Our data demonstrate that the key interactions in the bound structures are found between the conserved carbapenem core (β-lactam and pyrrole rings and the exocyclic sulfur) of the antibiotic and the divalent zinc ions, as well as the backbone and sidechain residues of the IMP-13 active site, particularly the L1 and L3 loops. Notably fewer interactions are made with the antibiotic tail region, leading to high flexibility, which likely affects enzyme efficiency, rendering careful design of the tail section key in drug discovery efforts. That IMP-13 is not selective towards the antibiotic tail region likely contributes to its broad-spectrum activity, which makes the B1 class metallo-β-lactamases particularly challenging resistance determinants. A key feature of the binding mode is the interaction between the tryptophan of L1 and the carbapenem scaffold – the tryptophan forms a closed tunnel over the β-lactam ring, thus locking the loop and the antibiotic in place (Fig. 1D). In the apo-state crystal structures, two positions for the L1 loop are observed, open and closed. Molecular dynamics simulations also show different degrees of flexibility in the L1 loop region. These results are supported by the fast-timescale motion for loop L1 observed in the apo form in the hetNOE experiment, which is reduced in the presence of the antibiotic ertapenem (Fig. 5), and in particular the substantial reduction in the flexibility of Trp28HεNε between the apo and ertapenem-bound states. These observations are consistent with previous NMR studies on a sub-class B1 di-zinc metallo β-lactamase from *Bacteroides fragilis* (54-56), where L1 loop residues show lower hetNOE values in the free-form compared to in the presence of a tight-binding inhibitor, most notably for the L1 tryptophan indole (Trp28 for IMP-13, Trp49 in (56)), indicating a potentially important role of the L1 loop in substrate recruitment and stabilization during the hydrolysis reaction. Previous studies have discussed whether the tryptophan and other hydrophobic residues in the L1 loop could act as a

Antimicrobial Agents and Chemotherapy
AAC
Antimicrobial Agents and Chemotherapy
Downloaded from http://aac.asm.org/ on April 2, 2020 at GSF/ZENTRALBIBLIOTHEK

Accepted Manuscript Posted Online

Antimicrobial Agents and Chemotherapy

AAC

Antimicrobial Agents and Chemotherapy

Downloaded from http://aac.asm.org/ on April 2, 2020 at GSF/ZENTRALBIBLIOTHEK

342 recruiter, loosely binding the substrate in the open formation and then moving to the closed
343 formation to aid substrate addition to the binding site (54, 56).

344 Nevertheless, it is clear from the MD simulations (Fig. 3) that differences in antibiotic structure affect
345 the restriction of the L1 loop, with doripenem, ertapenem and meropenem complexes showing the
346 greatest restriction in the L1 loop mobility. This is consistent with kinetic parameters reported for
347 IMP-13 (SI Table 2), showing tight binding for meropenem and ertapenem (K_{m} in the low µM and
348 high nM range respectively). In contrast imipenem shows weaker binding (ca. 50 µM), consistent
349 with the higher L1 flexibility. Notably the k_{cat} for imipenem is two orders of magnitude higher than
350 meropenem and ertapenem. Given that product release, preceded by the necessary L1 opening,
351 likely determines the turnover rate, this indicates that tighter binding reduces the turnover rate of
352 IMP-13. Consequently an efficient, non-covalent inhibitor could interact with and stabilize the L1
353 loop in the closed conformation forming a principle for inhibitor design.

354 IMP-13 shows 83% and 92% sequence identity with the IMP-1 and IMP-2 forms respectively and is
355 quite divergent from other variants (41). Consequently, it is instructive to compare our structures to
356 other available MBL structures (Fig. 6, SI10).

357 Comparison of the IMP-1 structures (PDB: 5Y5B, 5EV6 (58)) with both our $\mathrm{apo}_{\mathrm{closed}}$ and carbapenem-
358 bound IMP-13 structures yields differences in the L1 region. The amino acid sequences are highly
359 conserved between L1 regions of the two, with only one difference at the C-terminal end of the loop
360 (IMP-1 Pro32 changed to Thr in IMP-13). In one of the IMP-1 structures, the β-strand of the loop at
361 this point is seen to be straighter and further out from the active site than in the case of our
362 presented structures, despite the tip of the loop being closer to the active site than in the open-
363 conformation IMP-13 structure presented here. It is likely that the Pro32 to Thr mutation leads to a
364 more flexible loop in IMP-13 and more restricted loop in IMP-1, as a result of the more constrained
365 dihedral angles of proline. Mutagenesis analysis of IMP-18 (59) (subclass B4 β-lactamase (31)) also
366 indicates that this residue has a key effect as turnover rates of the enzyme are significantly altered

Accepted Manuscript Posted Online

Antimicrobial Agents and Chemotherapy

AAC

Antimicrobial Agents and Chemotherapy

(3 and 10-fold increase in k_{cat} for imipenem and meropenem respectively) on mutation from threonine to proline. IMP-2 also lacks Pro32 at the end of L1, which is instead mutated to Ser. The IMP-2 structure (4UBQ (60)) shows that the loop is found between the apo_{open} and apo_{closed} structures reported here. The varying extent of the β-strand structure (B2 and B3) on either side of the L1 loop may reflect the dynamic nature of this protein part and thus the loop can be captured in different conformations in different crystal structures.

The ligands crystallized previously with IMP-1 belong to different compound classes and hence we compare with our carbapenem-bound structures to identify if similar interactions are exploited Comparison with the IMP-1 structure bound to the mercaptocarboxylate inhibitor (57) (PDB: 1DD6) shows that the benzyl ring is pointing towards the loop (residues 21–23). Were the loop in the same position as in IMP-13, this would clash with the loop position, particularly with Val31. The position of the loop in IMP-1 is shifted laterally by approximately 1 Å. This could indicate potential binding selectivity to IMP-1 or an alternative explanation of sterically-induced loop movement. The free thiol of mercaptocarboxylate is coordinated by the two zinc atoms, displacing the nucleophilic water, equivalent to the carboxylate of β-lactams. In contrast both the tertiary amine and the sulfur of the thiophene ring point in the opposite orientation to comparable antibiotic residues. This suggests further structural optimization, based on a knowledge of antibiotic binding, could be used to optimize inhibitor interactions.

Structures of bisthiazolidine inhibitors bound to IMP-1 (PDB: 5EWA) (58) show a number of interactions mimicking those of antibiotic binding. The free thiol is coordinated by Zn1 and Zn2, displacing the nucleophilic water, while the thiazoline rings interact with the L1 tryptophan creating stacking interactions. The carboxylate interacts with the lysine residue in L3, equivalent to the β-lactam carboxylate. In contrast a phosphonate inhibitor (61) (PDB: 5HH4) does not displace the nucleophilic water, with the phosphonate group coordinating Ser119 (IMP-1 numbering) and the nucleophilic water. The pyridine nitrogen and carboxylate interact with Zn2 and the L3 lysine, again

Downloaded from http://aac.asm.org/ on April 2, 2020 at GSF/ZENTRALBIBLIOTHEK

Accepted Manuscript Posted Online

Antimicrobial Agents and Chemotherapy

AAC

Antimicrobial Agents and Chemotherapy

making interactions similar to those observed in our antibiotic-bound structures. The pyridine ring makes a T-shaped π-stacking interaction with the L1 tryptophan. These comparisons suggest that mimicking key interactions found in the antibiotic complex structures presented in this paper is important in designing inhibitors.

Comparing our IMP-13 structures to NDM-1 β-lactamase, another broad-spectrum MBL of clinical relevance, the key difference is the replacement of the tryptophan of L1 (Trp28) in IMP-13 with a phenylalanine in all 17 NDM variants (62). Consequently, this suggests an alternative mode of binding. In the published structure of NDM-1 in complex with hydrolyzed meropenem (PDB: 4EYL, re-refined in 5N0H) (63), the loop is shown in the open conformation, and therefore does not form a closed tunnel covering the β-lactam ring. In contrast Trp28 of IMP-13 shows direct interactions with the bound carbapenems, whilst the equivalent Phe70 of NDM-1 is more than 7 Å away and does not interact with the ligand. The conservation of this residue in all known NDM-1 variants indicates the importance of this amino acid for the proteins' activity. The equivalent residues to Val25 (Met in NDM-1), which in IMP-13 flanks the flexible loop section and interacts with C21 of meropenem, is seen in NDM-1 in a location where this interaction is removed altogether. The equivalent of Val31, the other flanking valine, is also seen in an altered position. This is further away from C21 of the antibiotic but is closer to the methylamine group, which could explain why this group of the meropenem molecule is in a different location in this structure, differing in position by around 5 Å.

We extended our comparison to structures of a variety of NDM proteins bound to various ligands that were deposited in the PDB in 2017 and 2018 (PDBs: 4TYF, 4TZ9, 4TZB, 4TZE, 4TZF, 5WIG (64), 5WIH (64), 5XP9 (65), 5A5Z (66), 5N0H (67), 5N0I , 5YPK (46), 5YPL (46) , 5YPN (46), 6EX7 (67), 5YPM (46), 5JQJ, 5K4M, 5XP6 (65)). Notably, none of these structures show a fully "closed-tunnel" conformation, as seen in the IMP-13-carbapenem complexes presented here. The backbone is seen in a half-closed formation in many of these PDBs (e.g. 5JQJ, 5K4M, 5XP6), but the chain never fully reaches over the substrate. This could lead to a reduced contact area between the ligand and the

Downloaded from http://aac.asm.org/ on April 2, 2020 at GSF/ZENTRALBIBLIOTHEK

Accepted Manuscript Posted Online

Antimicrobial Agents and Chemotherapy

AAC

Antimicrobial Agents and Chemotherapy

Downloaded from http://aac.asm.org/ on April 2, 2020 at GSF/ZENTRALBIBLIOTHEK

417 protein. The reduced hydrophobicity of this loop in NDM-1 could also explain the higher K_m (lower
418 affinity) of meropenem and imipenem (SI Table 2) relative to that of the IMP enzymes (28).

419 We also compare our results to the natural target of β-lactam antibiotics, the penicillin binding
420 proteins. A structure of Penicillin Binding Protein 3 (68) (PBP-3) bound to meropenem is available,
421 facilitating comparison between the interactions of meropenem with a β-lactam target protein (PBP)
422 and the enzymes (β-lactamases) that degrade it (Fig. 7). From the point of view of drug development,
423 comparative studies could highlight key similarities and differences, aiding with development of new
424 antibiotics in this class with lower susceptibility to the β-lactamase-driven degradation. The major
425 interactions, primarily hydrophobic, between the protein and the antibiotic are maintained, but key
426 differences are observed. Firstly, the central Trp28 interaction of IMP-13, both to the sulfur and to
427 C21 of the core carbapenem scaffold, is replaced by a hydrophobic interaction with Phe533 of PBP-3.
428 The interactions from His139 on L3 are partially emulated in PBP-3 by Gly486, whilst Asn167 and
429 Cys158 provide interactions similar to Thr487 and Lys484 of PBP-3 respectively. However, whilst
430 these interactions are different, they are very similar in character. It is also interesting to note the
431 difference between the meropenem and imipenem interactions. In PBP, the imipenem scaffold
432 (lacking C21) interacts with Tyr532, whilst C21 of meropenem displaces this and Phe533 rotates by
433 180° around the chain to form an alternative hydrophobic environment in the vicinity. Despite the
434 strong Tyr interaction, and the fact that this is closer to the native position than in the meropenem-
435 bound form, the imipenem binds a factor of 16 times weaker than meropenem (68), indicating that
436 the tail plays a much stronger role in the binding to PBP than to IMP-13, where the carbapenem
437 scaffold and alterations to it are more important. PBP-3 binding also utilizes an intricate water
438 network to align for formation of the covalent bond with Ser294 that ultimately deactivates the
439 protein. Neither covalent interactions nor a water network are seen in the IMP-13 or NDM-1
440 structures. The similarities at play highlight the challenge that drug discovery programmes face in
441 this area, but the differences may provide opportunities that can be exploited to deliver novel
442 pharmaceutical solutions.

Accepted Manuscript Posted Online

Antimicrobial Agents and Chemotherapy

AAC

Antimicrobial Agents and Chemotherapy

Downloaded from http://aac.asm.org/ on April 2, 2020 at GSF/ZENTRALBIBLIOTHEK

443 We report high-resolution structures of IMP-13 in diverse functional states and with different ligands
444 bound. The structures explain the specificity of the enzymatic mechanism and molecular recognition
445 of substrates by the IMP-13 β-lactamase. The data presented and the comparisons above suggest
446 that in IMP-13 the active-site loop plays a central role in antibiotic binding, with the primary
447 interactions to the core carbapenem scaffold. Consequently, such identified motifs that cause
448 restriction in the L1 loop flexibility could form important parts of β-lactamase inhibitors engaging
449 and stabilizing the loop in the closed conformation and blocking access of the natural substrates. The
450 substantial chemical shift changes observed by NMR in the tryptophan indole region (Fig. 4, SI7)
451 could be used in high-throughput screening to identify ligands with the potential to stabilize the
452 active-site loop in the closed conformation, similar to previous 2D screening approaches focusing on
453 spectral properties specific to the system of interest (69).

454 On the other hand, the ability of the loop to adopt a fully-open state, as observed in the apo_{open}
455 structure of IMP-13 provides an alternative strategy for inhibitor development. Most drug
456 development strategies on these targets have so far been aimed at the active site itself. As the loop
457 appears to play an active role in the binding of ligands to the protein, prevention of the loop closing
458 by an allosteric inhibitor could have a similar inhibitory effect.

459 The presented crystal structures and experimental NMR data combined with our molecular
460 dynamics simulations provide complementary information about changes in conformational
461 dynamics linked to ligand binding that should be considered in the development of small molecule
462 inhibitors.

463

Accepted Manuscript Posted Online

Antimicrobial Agents and Chemotherapy

AAC

Antimicrobial Agents and Chemotherapy

Downloaded from http://aac.asm.org/ on April 2, 2020 at GSF/ZENTRALBIBLIOTHEK

Materials and Methods

Protein expression and purification

The mature form of IMP-1 (residues 29-276) and IMP-13 (residues 21-246) proteins without signal peptide were cloned into a pET-SUK vector (70). The constructs were transformed into *E. coli* BL21 (DE3) cells and plated on LB agar supplemented with Kanamycin (50 µg/ml). Cells were grown in ZYM 5052 autoinduction medium (71) at 37 °C until an OD_{600} of 2.0 and thereafter protein was expressed at 20 °C overnight. The cells were collected by centrifugation, resuspended in lysis buffer (50 mM Tris-HCl pH 8.0, 300 mM NaCl, 5 mM β-Mercaptoethanol, 20 mM imidazole supplemented with AEBSF, DNase I and lysozyme) and lyzed by sonication. The lysate was clarified by centrifuging for 45 minutes at 27,000 rpm and the pH was adjusted to 8.0. The resulting supernatant was then passed twice over a HisTrap-excel column (GE healthcare) pre-equilibrated with lysis buffer. The column was washed with binding buffer (50 mM Tris-HCl pH 8.0, 300 mM NaCl, 5 mM β-mercaptoethanol, 20 mM imidazole, 10 mM $ZnCl_2$) and protein was eluted with elution buffer (50 mM Tris-HCl pH 8.0, 300 mM NaCl, 5 mM β-Mercaptoethanol, 300 mM imidazole). SUMO hydrolase (dtUD1, (72) provided by Protein Expression and Purification Facility (PEPF), Helmholtz Zentrum München) was added to the eluted protein, gently mixed and incubated for one hour at room temperature followed by buffer exchange to binding buffer. A second step of affinity chromatography was performed to remove the SUMO-tag and SUMO protease. IMP-1/13 containing fractions were then concentrated and purified to homogeneity using Superdex 75 size exclusion column pre-equilibrated with 5 mM Tris pH 8.0, 50 mM NaCl, 5 mM β-mercaptoethanol and 10 µM $ZnCl_2$.

For isotopically-labelled expression, cells were grown in M9 minimal medium supplemented with $^{15}NH_4Cl$ and ^{13}C-glucose and induced as above at an OD_{600} of 1, with overnight expression at 20 ˚C. Cells were collected by centrifugation and resuspended in lysis buffer (100 mM Tris, 300 mM NaCl, 5 mM β-Mercaptoethanol, pH 8.0) supplemented with DNAse I and AEBSF. The supernatant was

Accepted Manuscript Posted Online

Antimicrobial Agents and Chemotherapy

AAC

Antimicrobial Agents and Chemotherapy

Downloaded from http://aac.asm.org/ on April 2, 2020 at GSF/ZENTRALBIBLIOTHEK

passed twice over ZnNTA beads. In our hands, NDM-1 was observed (by paramagnetic effects in NMR spectra) to bind Ni from the column in its active site; therefore, to prevent the possibility of the same occurring with IMP-13 and affecting the spectral quality, the NTA beads were loaded with Zn to ensure the IMP-13 metal binding site was loaded with Zn. The column was pre-equilibrated with lysis buffer as above and SUMO hydrolase added to the protein on the column and left overnight at room temperature. The cleaved IMP-13 was eluted with 5 ml lysis buffer and further purified using Superdex 75 size exclusion chromatography pre-equilibrated with NMR buffer (50 mM HEPES, 100 mM NaCl, pH 7.0). Samples were supplemented with 10% D_2O for NMR spectroscopy.

Crystallization of IMP-13 in apo and carbapenem-bound forms

Purified protein was concentrated to 12 mg/ml and screening for crystallization conditions was performed using commercially available buffer sets in a sitting-drop vapor diffusion setup by mixing 0.2 µl of protein complex solution and 0.2 µl of buffer solution. For co-crystallization, meropenem and doripenem powder was added to protein solution (100 and 50 mM final concentration, respectively) and incubated for 30 minutes. For co-crystallization of IMP-13 with ertapenem and imipenem, antibiotic powder was dissolved in crystallization buffer and mixed with protein to final concentration of 5 and 25 mM, respectively. All crystals were obtained at room temperature from solutions containing 0.1 M Tris pH 8.5, 25% PEG 4000 (apo_{open}, **PDB ID: 6R79** - loop open), 0.1 M SPG buffer pH 8.0, 25% PEG 1500 (apo_{closed}, **PDB ID: 6R78** - loop closed), 0.1 M Bis-Tris pH 6.5, 25% PEG 3350 (meropenem complex, **PDB ID: 6R73**), 0.1 M Bis-Tris pH 5.5, 0.2 M Ammonium sulfate, 25% PEG 3350 (imipenem complex, **PDB ID: 6RZR**), 0.1 M tri-Sodium acetate pH 5.6, 0.2 M Ammonium acetate, 30% PEG 4000 (ertapenem complex, **PDB ID: 6RZS**) and 0.1 M Sodium HEPES pH 7.5, 25% PEG 2000 MME (doripenem complex, **PDB ID: 6S0H**).

Structure determination and refinement

Crystals were cryo-protected in 20% glycerol (apo), MPD (meropenem complex) or 25% ethylene glycol (imipenem, ertapenem and doripenem complexes) in the mother liquor and flash-frozen in

Accepted Manuscript Posted Online

Antimicrobial Agents and Chemotherapy

AAC

Antimicrobial Agents and Chemotherapy

liquid nitrogen. The diffraction data were collected at the id30b beamline at ESRF (Grenoble, France) and on the X06SA beamline at the Swiss Light Source (Paul Scherrer Institut, Villigen, Switzerland). The data were indexed and integrated using XDS (73, 74), and scaled and merged using Aimless (75). The initial phases were obtained by molecular replacement calculated using Phaser (76) and the IMP-1 structure as a search model (PDB 1DD6 (57)). The initial model was manually rebuilt according to the resulting electron density maps using Coot (77). Structures of IMP-13 in complex with hydrolyzed carbapenems were solved using the same approach and the IMP-13 apo structure as a search model. Carbapenem geometrical restraints files were created using the Grade web server (78). Restrained refinement was performed using Phenix, or Refmac with additional restraints generated using proSMART (79-81). Five percent of the reflections were used for cross-validation analysis and the R_{free} was employed to monitor the refinement strategy. Water molecules were added using Coot and afterwards manually inspected. The final models were deposited in the Protein Data Bank under accession numbers 6R79 and 6R78 for apo and 6R73, 6RZR, 6RZS and 6S0H for meropenem, imipenem, ertapenem and doripenem bound forms, respectively. Interactions were visualized with BIOVIA Discovery Studio Visualiser (82). All molecular graphics were prepared using PyMOL (83) or Maestro (84). Crystallographic parameters are shown in SI Table 4.

NMR spectroscopy

NMR experiments were recorded at 298 K on Bruker Avance III 600 MHz and 800 MHz spectrometers (^{1}H frequency 600 or 800 MHz respectively) equipped with a 5 mm TCI or QCI cryoprobe. For assignments ^{1}H,^{15}N HSQC, and 3D ^{15}N-edited NOESY, HNCA, HN(CO)CA, HNCACB, HN(CO)CACB and CBCACONH experiments were recorded on uniformly ^{15}N,^{13}C-labelled samples. Samples at 0.5–0.6 mM were prepared in NMR buffer (50 mM HEPES, 100 mM NaCl, pH 7.0) supplemented with 10% D_2O. For the ertapenem assignment, the sample was supplemented with 5.7 mM ertapenem (ca. 10-fold excess). Spectra were recorded with 2.9 mM and 5.7 mM ertapenem added and with no further changes observed between the two spectra, the protein was assumed to

Downloaded from http://aac.asm.org/ on April 2, 2020 at GSF/ZENTRALBIBLIOTHEK

Accepted Manuscript Posted Online

Antimicrobial Agents and Chemotherapy

AAC

Antimicrobial Agents and Chemotherapy

Downloaded from http://aac.asm.org/ on April 2, 2020 at GSF/ZENTRALBIBLIOTHEK

be saturated. Backbone assignment experiments (excepting the 3D NOESY) were recorded with 25% non-uniform sampling, using Poisson-gap sampling (85), and reconstructed using the Cambridge CS package using the CS-IHT algorithm (86). Heteronuclear NOE experiments were recorded at 600 MHz and 298 K using a sequence with interleaved saturated and unsaturated planes (53). Spectra were acquired with 2048 x 300 complex points and a recycle delay of 1.2 s, with 32 scans. NOEs were calculated as the ratio of saturated to unsaturated experiments. Errors were calculated using the standard deviation of the noise. All spectra were processed with zero-filling and Gaussian and/or sinebell window functions in the direct dimension and a sinebell window function in the indirect dimension. The water signal was removed by convolution with a sine function. Spectra were processed in Azara (W. Boucher, unpublished) and analyzed using CCPN Analysis (87). Chemical shift perturbations were calculated according to the formula: $\Delta\delta = \sqrt{\left((\Delta\delta_{\mathrm{HN}})^2 + \left(\Delta\delta_{15_{\mathrm{N}}}\right)^2/6\right)}$.

Antibiotic hydrolysis assay

Enzymatic studies were carried out on the expressed proteins to confirm that the protein was in its active state. The enzymatic activity of the recombinantly produced metallo-β-lactamases was monitored as previously described (88) at 37 °C in 75mM HEPES buffer at pH 7.3, using 1-500 µM meropenem or imipenem respectively, as substrate. β-lactam hydrolysis was followed at 300 nm (SI Table 2).

Molecular dynamics simulations

Simulations were run using Maestro Desmond Molecular Dynamics Package version 2017.3 (89, 90). PDBs of the apo_{closed} and complex structures were prepared adding missing sidechains and hydrogens using YASARA Structure's built-in *clean* command (91). Structures were then imported into Schrödinger Maestro version 2017.3 and further refined using the Maestro version 11.1 'Protein Preparation Wizard'(92). Protonation states were calculated using PROPKA (93, 94) at pH 7.0 ± 2.0 and minimization of hydrogen positions with restrained backbone was performed using OPLS3 force

Accepted Manuscript Posted Online

Antimicrobial Agents and Chemotherapy

AAC

Antimicrobial Agents and Chemotherapy

field (95) in order to optimize the hydrogen bonding network. Both apo_{closed} and complex systems were then prepared for simulation using Maestro version 11.1 'System Builder' GUI using TIP4P (96) solvent model (crystallographic water molecules were deleted) in an automatically generated cubic cell with periodic boundary conditions. In addition to the solvated complex, Na^+ and Cl^- ions corresponding to a 150 mM buffer were placed in the cell in order to set the total net charge to zero. The coordination of the zinc metal centers was maintained by adding pseudo-bonds between the metals and the coordinating residues, using the default parameters for angles and charges of the OPLS-AA 2005 force field for the sake of the speed of the calculations. In the case of the apo protein, a tetrahedral coordination was chosen for both the zinc atoms in the active site. Furthermore, in the apo structure, no pseudo-bond was added to the bridging water molecule observed in the crystallographic structure, thus reducing the coordination of the metal centers to three residues to simulate the hydration sphere around the zinc atoms. For all the other complexes, the geometry of the zinc bound to histidines was considered tetrahedral (with a coordination number of four) and the other zinc atom was considered to be octahedral (with a coordination number of six).

Simulations of the systems were run using Maestro 'Molecular Dynamics' Desmond GUI for a total simulation time of 50 ns to ensure system convergence (this was checked on the RMSD plot of the simulations), recording intervals every 50 ps (1000 snapshots in total) for xyz coordinates and 1.2 ps for potential energy calculations of the ensemble. Replicates of the simulations were performed using the Desmond molecular dynamics package version 2019.3 in Maestro v11.8. One replica for each system was simulated for 100 ns, recording intervals every 100 ps (1000 snapshots in total) for xyz coordinates and 2.5 ps for potential energy calculations. For both the first run of production MD and for the replicates, the ensembles were set to constant temperature (300 K) and pressure (1.01 bar); the force cut-off radius was set to 9.0 Å and each solvated model was relaxed with Desmond default relaxation protocol before starting the simulation. Simulations were performed on a standard PC workstation (Intel Core i7 5960x, 32 GB RAM) using Nvidia GeForce 1070 GPU.

Downloaded from http://aac.asm.org/ on April 2, 2020 at GSF/ZENTRALBIBLIOTHEK

Accepted Manuscript Posted Online

Accession Numbers

Coordinates and structure factors have been deposited in the Protein Data Bank with accession codes PDB: 6R79 - apo loop open; 6R78 - apo loop closed; 6R73 - meropenem complex; 6RZR - imipenem complex; 6RZS - ertapenem complex; 6S0H - doripenem complex. NMR assignments have been deposited in the BMRB: 50012 - apo; 50013 - ertapenem-bound.

Acknowledgements

This project was carried out with the support of BAG proposal MX-2088 at the ESRF Grenoble. We are grateful to the Protein Expression and Purification Facility and the X-ray Crystallography Platform at Helmholtz Zentrum München for support. We are thankful for all the discussion and help in structure refinement during the 2019 CCP4/APS School in Macromolecular Crystallography. We are also grateful to Dr. Rita Monson for useful discussions. C.S., R.F., G.M.P. and M.S. acknowledge funding from the European Union's Framework Programme for Research and Innovation Horizon 2020 (2014-2020) under the Marie Skłodowska-Curie Grant Agreement No. 675555, Accelerated Early staGe drug discovery (AEGIS). M.B. is supported by Helmholtz Zentrum München. M.K. is supported by Wrocław Centre of Biotechnology program, The Leading National Research Centre (KNOW) for years 2014–2018and by a doctoral fellowship by the National Science Center (NCN, Poland), grant no 2018/28/T/NZ1/00337. R.M.N. and K.Z .are supported by the German Federal Ministry of Research and Education (BMBF) program "Targetvalidierung für die pharmazeutische Wirkstoffentwicklung", grant no. GFTARV38.

Author contributions

C.S., K.Z., M.B., R.Z. and M.K. carried out molecular biology, protein expression and purification. C.S., K.Z., M.K. and R.Z carried out crystallisation, data acquisition and analysis and M.B. carried out NMR

Antimicrobial Agents and Chemotherapy
AAC
Antimicrobial Agents and Chemotherapy
Downloaded from http://aac.asm.org/ on April 2, 2020 at GSF/ZENTRALBIBLIOTHEK

Accepted Manuscript Posted Online

Antimicrobial Agents and Chemotherapy

AAC

Antimicrobial Agents and Chemotherapy

measurements and analysis. R.M. carried out enzymatic assays and R.F. performed molecular dynamics simulations. C.S., M.B. and K.Z prepared the manuscript. H.M., M.S. and G.P. supervised the project.

Declaration of Interests

The authors declare no competing interests.

Downloaded from http://aac.asm.org/ on April 2, 2020 at GSF/ZENTRALBIBLIOTHEK

Accepted Manuscript Posted Online

Antimicrobial Agents and Chemotherapy

AAC

Antimicrobial Agents and Chemotherapy

Downloaded from http://aac.asm.org/ on April 2, 2020 at GSF/ZENTRALBIBLIOTHEK

References

1. **Exner M, Bhattacharya S, Christiansen B, Gebel J, Goroncy-Bermes P, Hartemann P, Heeg P, Ilschner C, Kramer A, Larson E, Merkens W, Mielke M, Oltmanns P, Ross B, Rotter M, Schmithausen RM, Sonntag H-G, Trautmann M.** 2017. Antibiotic resistance: What is so special about multidrug-resistant Gram-negative bacteria? GMS Hyg Infect Control **12:**Art5.
2. **Bush K.** 2010. Bench-to-bedside review: The role of β-lactamases in antibiotic-resistant Gram-negative infections. Critical care **14:**224.
3. **Tooke CL, Hinchliffe P, Bragginton EC, Colenso CK, Hirvonen VHA, Takebayashi Y, Spencer J.** 2019. β-Lactamases and β-Lactamase Inhibitors in the 21st Century. J Mol Biol **431:**3472-3500.
4. **Pitout JDD, Sanders CC, Sanders Jr WE.** 1997. Antimicrobial Resistance with Focus on β-Lactam Resistance in Gram-Negative Bacilli. Am J Med **103:**51-59.
5. **Mölstad S, Lundborg CS, Karlsson A-K, Cars O.** 2002. Antibiotic Prescription Rates Vary Markedly Between 13 European Countries. Scandinavian Journal of Infectious Diseases **34:**366-371.
6. **Waxman D, Strominger JL.** 1983. Penicillin-binding proteins and the mechanism of actions of the β-lactam antibiotics. Annual Reviews Biochemistry **52:**825-869.
7. **Fleming A.** 1929. On the antibacterial action of cultures of a penicillium, with special reference to their use in the isolation of *B. Influenzae*. British Journal of Experimental Pathology **10:**226-236.
8. **Gaynes R.** 2017. The Discovery of Penicillin—New Insights After More Than 75 Years of Clinical Use. Emerging Infect Dis **23:**849-853.
9. **Drawz SM, Bonomo RA.** 2010. Three decades of β-lactamase inhibitors. Clinical Microbiology Reviews **23:**160-201.
10. **Crowder MW, Spencer J, Vila AJ.** 2006. Metallo-β-lactamases: Novel Weaponry for Antibiotic Resistance in Bacteria. Accounts of Chemical Research **39:**721-728.

Accepted Manuscript Posted Online

11. **Palumbi SR.** 2001. Humans as the World's Greatest Evolutionary Force. Science **293:**1786-1790.

12. **Abraham EP, Newton GGF, Hale CW.** 1954. Purification and some properties of cephalosporin N, a new penicillin. Biochemical journal **58:**94-102.

13. **Newton GG, Abraham EP.** 1956. Isolation of cephalosporin C, a penicillin-like antibiotic containing D-α-aminoadipic acid. Biochemical journal **62:**651-658.

14. **Birnbaum J, M.Kahan F, Kropp H, MacDonald JS.** 1985. Carbapenems, a new class of β-lactam antibiotics. Discovery and development of imipenem/cilastatin. Am J Med **78:**3-21.

15. **Senda K, Arakawa Y, Ichiyama S, Nakashima K, Ito H, Ohsuka S, Shimokata K, Kato N, Ohta M.** 1996. PCR Detection of Metallo-β-Lactamase Gene (blaIMP) in Gram-Negative Rods Resistant to Broad-Spectrum β-Lactams. Journal of Clinical Microbiology **34:**2909–2913.

16. **Livermore D.** 1995. β-lactamases in laboratory and clinical resistance. Clinical Microbiology Reviews **8:**557-584.

17. **WHO.** 27 Feb 2017 WHO priority pathogens list for R&D of new antibiotics: www.who.int/medicines/publications/WHO-PPL-Short_Summary_25Feb-ET_NM_WHO.pdf?ua=1.

18. **Bush K, Jacoby GA, Medeiros AA.** 1995. A Functional Classification Scheme for β-Lactamases and Its Correlation with Molecular Structure. Antimicrobial Agents and Chemotherapy **39:**1211–1233.

19. **Meini M-R, Llarrull LI, Vila AJ.** 2015. Overcoming differences: the catalytic mechanism of metallo-β-lactamases. FEBS Lett**:**3419-3432.

20. **Ito H, Arakawa Y, Ohsuka S, Wacharotayankun R, Kato N, Ohta M.** 1995. Plasmid-Mediated Dissemination of the Metallo-β-Lactamase Gene blaIMP among Clinically Isolated Strains of *Serratia marcescens*. Antimicrobial Agents and Chemotherapy **39:**824–829.

Antimicrobial Agents and Chemotherapy

AAC

Antimicrobial Agents and Chemotherapy

Downloaded from http://aac.asm.org/ on April 2, 2020 at GSF/ZENTRALBIBLIOTHEK

Accepted Manuscript Posted Online

21. **Santella G, Pollini S, Docquier J-D, Mereuta AI.** 2010. Intercontinental Dissemination of IMP-13-Producing *Pseudomonas aeruginosa* Belonging in Sequence Type 621. Journal of Clinical Microbiology **48:**4342–4343.

22. **Neu HC, Fu KP.** 1978. Clavulanic Acid, a novel inhibitor of β-lactamases. Antimicrob Agents Chemother **14:**650-655.

23. **Ehmann DE, Jahić H, Ross PL, Gu R-F, Hu J, Kern G, Walkup GK, Fisher SL.** 2012. Avibactam is a covalent, reversible, non–β-lactam β-lactamase inhibitor. Proc Natl Acad Sci USA **109:**11663-11668.

24. **van Duin D, Bonomo RA.** 2016. Ceftazidime/Avibactam and Ceftolozane/Tazobactam: Second-generation β-Lactam/β-Lactamase Inhibitor Combinations. Clin Infect Dis **63:**234-241.

25. **Humphries RM, Yang S, Hemarajata P, Ward KW, Hindler JA, Miller SA, Gregson A.** 2015. First Report of Ceftazidime-Avibactam Resistance in a KPC-3-Expressing *Klebsiella pneumoniae* Isolate. Antimicrob Agents Chemother **59:**6605-6607.

26. **Mojica MF, Bonomo RA, Fast W.** 2016. B1-metallo-β-lactamases: where do we stand? Curr Drug Targets **17:**1029-1050.

27. **Lauretti L, Riccio M, Mazzariol A, Cornaglia G, Amicosante G, Fontana R, Rossolini GM.** 1999. Cloning and characterization of blaVIM, a new integron-borne metallo-β-lactamase gene from a *Pseudomonas aeruginosa* clinical isolate. Antimicrob Agents Chemother **43:**1584-1590.

28. **Yong D, Toleman MA, Giske CG, Cho HS, Sundman K, Lee K, Walsh TR.** 2009. Characterization of a New Metallo-β-Lactamase Gene, blaNDM-1, and a Novel Erythromycin Esterase Gene Carried on a Unique Genetic Structure in *Klebsiella pneumoniae* Sequence Type 14 from India. Antimicrobial Agents and Chemotherapy **53:**5046–5054.

29. **Hong DJ, Bae IK, Jang I-H, Jeong SH, Kang H-K, Lee K.** 2015. Epidemiology and Characteristics of Metallo-β-Lactamase-Producing *Pseudomonas aeruginosa*. J Infect Chemother **47:**81-97.

Antimicrobial Agents and Chemotherapy
AAC
Antimicrobial Agents and Chemotherapy
Downloaded from http://aac.asm.org/ on April 2, 2020 at GSF/ZENTRALBIBLIOTHEK

Accepted Manuscript Posted Online

694 30. **Bush K.** 2018. Past and Present Perspectives on β-lactamases. Antimicrob Agents Chemother
695 **62:**e01076-01018.
696 31. **Zhao W-H, Hu Z-Q.** 2011. IMP-type metallo-β-lactamases in Gram-negative bacilli:
697 distribution, phylogeny, and association with integrons. Critical Reviews in Microbiology
698 **37:**214-226.
699 32. **Ho P-L, Lo W-U, Chan J, Cheung Y-Y, Chow K-H, Yam W-C, Lin C-H, Que T-L.** 2013. pIMP-
700 PH114 Carrying bla IMP-4 in a *Klebsiella pneumoniae* Strain is Closely Related to Other
701 Multidrug-Resistant IncA/C2 Plasmids. Curr Microbiol **68:**227-232.
702 33. **Mendes RE, Toleman MA, Ribeiro J, Sader HS, Jones RN, Walsh TR.** 2004. Integron Carrying
703 a Novel Metallo-β-Lactamase Gene, blaIMP-16, and a Fused Form of Aminoglycoside-
704 Resistant Gene aac(6')-30/aac(6')-Ib': Report from the SENTRY Antimicrobial Surveillance
705 Program. Antimicrob Agents Chemother **48:**4693-4702.
706 34. **Chen Z, Fang H, Wang L, Sun F, Wang Y, Yin Z, Yang H, Yang W, Wang J, Xia P, Zhou D, Liu C.**
707 2014. IMP-1 encoded by a novel Tn402-like class 1 integron in clinical *Achromobacter*
708 *xylosoxidans*, China. Sci Rep **4:**7212.
709 35. **Robert X, Gouet P.** 2014. Deciphering key features in protein structures with the new
710 ENDscript server. Nucleic Acids Res **42**.
711 36. **Pagani L, Colinon C, Migliavacca R, Labonia M, Docquier J-D, Nucleo E, Spalla M, Bergoli ML,**
712 **Rossolini GM.** 2005. Nosocomial Outbreak Caused by Multidrug-Resistant *Pseudomonas*
713 *aeruginosa* Producing IMP-13 Metallo-β-Lactamase. Journal of Clinical Microbiology
714 **43:**3824–3828.
715 37. **Queenan AM, Bush K.** 2007. Carbapenemases: the Versatile β-lactamases. Clinical
716 Microbiology Reviews **20:**440-458.
717 38. **Chouchani C, Marrakchi R, Henriques I, Correia A.** 2013. Occurrence of IMP-8, IMP-10, and
718 IMP-13 metallo-β-lactamases located on class 1 integrons and other extended-spectrum β-

Antimicrobial Agents and Chemotherapy
AAC
Antimicrobial Agents and Chemotherapy
Downloaded from http://aac.asm.org/ on April 2, 2020 at GSF/ZENTRALBIBLIOTHEK

Accepted Manuscript Posted Online

719 lactamases in bacterial isolates from Tunisian rivers. Scandinavian Journal of Infectious
720 Diseases **45:**95-103.
721 39. **Matsumura Y, Peirano G, Motyl MR, Adams MD, Chen L, Kresiwirth B, DeVinney R, Pitout**
722 **JDD.** 2017. Global molecular epidemiology of IMP-producing *Enterobacteriaceae*. Antimicrob
723 Agents Chemother **61:**e02729-02716.
724 40. **Bogaerts P, Bouchahrouf W, Lissoir B, Denis O, Glupczynski Y.** 2011. IMP-13-producing
725 *Pseudomonas monteilii* recovered in a hospital environment. Journal of Antimicrobial
726 Chemotherapy **66:**2434-2435.
727 41. **Santella G, Docquier J-D, Gutkind G, Rossolini GM, Radice M.** 2011. Purification and
728 Biochemical Characterization of IMP-13 Metallo-β-Lactamase. Antimicrobial Agents and
729 Chemotherapy **55:**399-401.
730 42. **Carfi A, Pares S, Duee E, Galleni M, Duez C, Frère J-M, Dideberg O.** 1995. The 3-D structure
731 of a zinc metallo-1-lactamase from *Bacillus cereus* reveals a new type of protein fold. The
732 EMBO Journal **14:**4914-4921.
733 43. **Garau G, García-Saez I, Bebrone C, Anne C, Mercuri P, Galleni M, Frere J-M, Dideberg O.**
734 2004. Update of the Standard Numbering Scheme for Class B β-Lactamases. Antimicrobial
735 Agents and Chemotherapy **48:**2347–2349.
736 44. **Borra PS, Samuelsen O, Spencer J, Walsh TR, Lorentzen MS, Leiros H-KS.** 2013. Crystal
737 Structures of *Pseudomonas aeruginosa* GIM-1: Active-Site Plasticity in Metallo-β-Lactamases.
738 Antibiotic Agents and Chemotherapy **57:**848-854.
739 45. **Brem J, Struwe WB, Rydzik AM, Tarhonskaya H, Pfeffer I, Flahman E, van Berkel SS,**
740 **Spencer J, Claridge TDW, McDonough MA, Benesch JLP, Schofield CJ.** 2014. Studying the
741 active-site loop movement of the São Paolo metallo-β-lactamase-1. Chem Sci**:**956-963.
742 46. **Feng H, Liu X, Wang S, Fleming J, Wang D-C, Liu W.** 2017. The mechanism of NDM-1-
743 catalyzed carbapenem hydrolysis is distinct from that of penicillin or cephalosporin
744 hydrolysis. Nature Communications **8**.

Antimicrobial Agents and Chemotherapy
AAC
Antimicrobial Agents and Chemotherapy
Downloaded from http://aac.asm.org/ on April 2, 2020 at GSF/ZENTRALBIBLIOTHEK

Accepted Manuscript Posted Online

47. **Page MI, Badarau A.** 2008. The Mechanisms of Catalysis by Metallo β-Lactamases. Bioinorganic Chemistry and Applications **2008:**1-14.

48. **Yamaguchi Y, Kuroki T, Yasuzawa H, Higashi T, Jin W, Kawanami A, Yamagata Y, Arakawa Y, Goto M, Kurosaki H.** 2005. Probing the Role of Asp-120(81) of Metallo-β-lactamase (IMP-1) by Site-directed Mutagenesis, Kinetic Studies, and X-ray Crystallography. J Biol Chem **280:**20824–20832.

49. **Lisa M-N, Palacios A, Aitha M, Gonzalez MM, Moreno DM, Crowder MW, Bonomo RA, Spencer J, Tierney DL, Llarrull LI, Vila AJ.** 2017. A general reaction mechanism for carbapenem hydrolysis by mononuclear and binuclear metallo-β-lactamases. Nature Communications **8**.

50. **Peri S, Steen H, Pandey A.** 2001. GPMAW - a software tool for analyzing proteins and peptides. Trends Biochem Sci **26:**687-689.

51. **Moali C, Anne C, Lamotte-Brasseur J, Groslambert S, Devreese B, Beeumen JV, Galleni M, Frere J-M.** 2003. Analysis of the Importance of the Metallo-β-Lactamase Active Site Loop in Substrate Binding and Catalysis. Chem Biol **10:**319-329.

52. **Jarymowycz VA, Stone MJ.** 2006. Fast Time Scale Dynamics of Protein Backbones: NMR Relaxation Methods, Applications, and Functional Consequences. Chemical Reviews **106:**1624-1671.

53. **Farrow NA, Muhandiram R, Singer AU, Pascal SM, Kay CM, Gish G, Steven E Shoelson, Pawson T, Forman-Kay JD, Kay LE.** 1994. Backbone dynamics of a free and phosphopeptide-complexed Src homology 2 domain studied by ^{15}N NMR relaxation. Biochemistry **33:**5984-6003.

54. **Scrofani SDB, Chung J, Huntley JJA, Benkovic SJ, Wright PE, Dyson HJ.** 1999. NMR Characterization of the Metallo-β-lactamase from *Bacteroides fragilis* and Its Interaction with a Tight-Binding Inhibitor: Role of an Active-Site Loop. Biochemistry **38:**14507-14514.

Antimicrobial Agents and Chemotherapy
AAC
Antimicrobial Agents and Chemotherapy
Downloaded from http://aac.asm.org/ on April 2, 2020 at GSF/ZENTRALBIBLIOTHEK

Accepted Manuscript Posted Online

55. **Huntley JJA, Scrofani SDB, Osborne MJ, Wright PE, Dyson HJ.** 2000. Dynamics of the Metallo-β-Lactamase from *Bacteroides fragilis* in the Presence and Absence of a Tight-Binding Inhibitor. Biochemistry **39:**13356-13364.

56. **Huntley JJA, Fast W, Benkovic SJ, Wright PE, Dyson HJ.** 2003. Role of a solvent-exposed tryptophan in the recognition and binding of antibiotic substrates for a metallo-β-lactamase. Protein Science **12:**1368-1375.

57. **Concha NO, Janson CA, Rowling P, Pearson S, Cheever CA, Clarke BP, Lewis C, Galleni M, Frere J-M, Payne DJ, Bateson JH, Abdel-Meguid SS.** 2000. Crystal Structure of the IMP-1 Metallo-β-Lactamase from *Pseudomonas aeruginosa* and Its Complex with a Mercaptocarboxylate Inhibitor: Binding Determinants of a Potent, Broad-Spectrum Inhibitor. Biochemistry **39:**4288-4298.

58. **Hinchliffe P, Gonzalez MM, Mojica MF, Gonzalez JM, Castillo V, Saiz C, Kosmopoulou M, Tooke CL, Llarrull LI, Mahler G, Bonomo RA, Vila AJ, Spencer J.** 2016. Cross-class metallo-β-lactamase inhibition by bisthiazolidines reveals multiple binding modes. Proc Natl Acad Sci USA **113:**e3745-e3754.

59. **Furuyama T, Nonomura H, Ishii Y, Hanson ND, Shimizu-Ibuka A.** 2016. Structural and Mutagenic Analysis of Metallo-β-Lactamase IMP-18. Antimicrobial Agents and Chemotherapy **60:**5521-5526.

60. **Yamaguchi Y, Matsueda S, Matsunaga K, Takashio N, Toma-Fukai S, Yamagata Y, Shibata N, Wachino J-i, Shibayama K, Arakawa Y, Kurosaki H.** 2015. Crystal Structure of IMP-2 Metallo-β-lactamase from Acinetobacter spp. Biol Pharm Bull **38:**96-101.

61. **Hinchliffe P, Tanner CA, Krismanich AP, Labbé G, Goodfellow VJ, Marrone L, Desoky AY, Calvopiña K, Whittle EE, Zeng F, Avison MB, Bols NC, Siemann S, Spencer J, Dmitrienko GI.** 2018. Structural and Kinetic Studies of the Potent Inhibition of Metallo-β-lactamases by 6-Phosphonomethylpyridine-2-carboxylates. Biochemistry **57:**1880-1892.

Antimicrobial Agents and Chemotherapy
AAC
Antimicrobial Agents and Chemotherapy
Downloaded from http://aac.asm.org/ on April 2, 2020 at GSF/ZENTRALBIBLIOTHEK

Accepted Manuscript Posted Online

795 62. **Khan AU, Maryam L, Zarrili R.** 2017. Structure, Genetics and Worldwide Spread of New Delhi
796 Metallo-β-Lactamase (NDM): a threat to public health. BMC Microbiol **17:**Article 101.
797 63. **King DT, Worrall LJ, Gruninger R, Strynadka NC.** 2012. New Delhi Metallo-β-Lactamase:
798 Structural Insights into β-Lactam Recognition and Inhibition. Journal of the American
799 Chemistry Society **134:**11362-11365.
800 64. **Stewart AC, Bethel CR, VanPelt J, Bergstrom A, Cheng Z, Miller CG, Williams C, Poth R,**
801 **Morris M, Laheel O, Nix J, Tierney DL, Page RC, Crowder MW, Bonomo RA, Fast W.** 2017.
802 Clinical Variants of New Delhi Metallo-β-lactamase are evolving to overcome zinc scarcity.
803 ACS Infections Diseases **3:**927-940.
804 65. **Wang R, Lai T-P, Gao P, Zhang H, Ho P-L, Woo PC-Y, Ma G, Kao RY-T, Li H, Sun H.** Bismuth
805 antimicrobial drugs serve as broad-spectrum metallo-β-lactamase inhibitors. Nature
806 Communications **9:**Article 439.
807 66. **Klingler F-M, Wichelhaus T, Frank D, Cuesta-Bernal J, El-Delik J, Muller HF, Sjuts H, Gottig S,**
808 **Koenigs A, Pos KM, Pogoryelev D, Proshak E.** 2015. Approved Drugs Containing Thiols as
809 Inhibitors of Metallo-β-lactamases: Strategy To Combat Multi-drug Resistant Bacteria.
810 Journal of Medicinal Chemistry **58:**3626-3630.
811 67. **Raczynska J, Shabalin I, Minor W, Wlodawer A, Jaskolski M.** 2018. A close look onto
812 structural models and primary ligands of metallo-β-lactamases. Drug Resistance Updates
813 **40:**1-12.
814 68. **Han S, Zaniewski RP, Marr ES, Lacey BM, Tomaras AP, Evdokimov A, Miller JR,**
815 **Shanmugasundaram V.** 2010. Structural basis for effectiveness of siderophore-conjugated
816 monocarbams against clinically relevant strains of *Pseudomonas aeruginosa*. Proc Natl Acad
817 Sci USA **107:**22002-22007.
818 69. **Jahnke W, Grotzfeld RM, Pellé X, Strauss A, Fendrich G, Cowan-Jacob SW, Cotesta S,**
819 **Fabbro D, Furet P, Mestan J, Marzinzik AL.** 2010. Binding or Bending: Distinction of

Antimicrobial Agents and Chemotherapy
AAC
Antimicrobial Agents and Chemotherapy
Downloaded from http://aac.asm.org/ on April 2, 2020 at GSF/ZENTRALBIBLIOTHEK

Accepted Manuscript Posted Online

Allosteric Abl Kinase Agonists from Antagonists by an NMR-based Conformational Assay. Journal of American Chemical Society **132:**7043-7048.

70. **Helmholtz Zentrum Muenchen Protein Expression and Purification Facility.** 2019. Bacterial Expression Vectors, Munich.

71. **Studier FW.** 2005. Protein production by auto-induction in high-density shaking cultures. Protein expression and purification **41:**207-234.

72. **Weeks SD, Drinker M, Loll PJ.** 2007. Ligation independent cloning vectors for expression of SUMO fusions. Protein expression and purification **53:**40-50.

73. **Kabsch W.** 2010. XDS. Acta Crystallographica **66:**125-132.

74. **Krug M, Weiss MS, Heinemann U, Mueller U.** 2012. XDSAPP: a graphical user interface for the convenient processing of diffraction data using XDS. Journal of Applied Crystallography **45:**568-572.

75. **Evans PE, Murshudov GN.** 2019. How good are my data and what is the resolution? Acta Crystallographica **69:**1204-1214.

76. **McCoy AJ, Grosse-Kunstleve RW, Adams PD, Winn MD, Storoni LC, Read RJ.** 2007. Phaser crystallographic software. Journal of Applied Crystallography **40:**658-674.

77. **Emsley P, Lohkamp B, Scott WG, Cowtan K.** 2010. Features and development of coot. Acta Crystallographica **66:**486-501.

78. **Smart OS, Womack TO, Sharff A, Flensburg C, Keller P, Paciorek W, Vonrhein C, Bricogne G.** 2011. Grade web server, Global Phasing Ltd., Cambridge, United Kingdom.

79. **Nicholls RA, Fischer M, McNicholas S, Murshudov GN.** 2014. Conformation-independent structural comparison of macromolecules with ProSMART. Acta Crystallographica **70:**2487-2499.

80. **Nicholls RA, Long F, Murshudov GN.** 2012. Low-resolution refinement tools in REFMAC5. Acta Crystallographica **68:**404-417.

Antimicrobial Agents and Chemotherapy

AAC

Antimicrobial Agents and Chemotherapy

Downloaded from http://aac.asm.org/ on April 2, 2020 at GSF/ZENTRALBIBLIOTHEK

Accepted Manuscript Posted Online

81. **Adams PD, Afonine PV, Bunkóczi G, Chen VB, Davis IW, Echols N, Headd JJ, Hung L-W, Kapral GJ, Grosse-Kunstleve RW, McCoy AJ, Moriarty NW, Oeffner R, Read RJ, Richardson DC, Richardson JS, Terwilliger TC, Zwarta PH.** 2010. PHENIX: a comprehensive Python-based system for macromolecular structure solution. Acta Crystallographica **66:**213-221.

82. **BIOVIA DS.** 2019. DiscoveryStudioVisualiser, San Diego: Dassault Systemes.

83. **Schrödinger.** Pymol Molecular Graphics System, Version 2.0 LLC, v1.8.

84. **Schrödinger.** 2017. L. L. C. Schrödinger Maestro Release 2017.3, New York, NY.

85. **Hyberts SG, Takeuchi K, Wagner G.** 2010. Poisson-Gap Sampling and Forward Maximum Entropy Reconstruction for Enhancing the Resolution and Sensitivity of Protein NMR Data. Journal of American Chemical Society **132:**2145-2147.

86. **Bostock MJ, Holland DJ, Nietlispach D.** 2012. Compressed sensing reconstruction of undersampled 3D NOESY spectra: application to large membrane proteins. Journal of Biomolecular NMR **54:**15-32.

87. **Vranken WF, Boucher W, Stevens TJ, Fogh RH, Pajon A, Llinas M, Ulrich EL, Markley JL, Ionides J, Laue ED.** 2005. The CCPN data model for NMR spectroscopy: development of a software pipeline. Proteins **59:**687-696.

88. **King AM, Reid-Yu SA, Wang W, King DT, Pascale GD, Strynadka NC, Walsh TR, Coombes BK, Wright GD.** 2014. Aspergillomarasmine A overcomes metallo-β-lactamase antibiotic resistance. Nature **510:**503-506.

89. **Bowers KJ, Chow DE, Xu H, Dror RO, Eastwood MP, Gregersen BA, Klepeis JL, Kolossvary I, Moraes MA, Sacerdoti FD, Salmon JK, Shan Y, Shaw DE.** 2006. Scalable Algorithms for Molecular Dynamics Simulations on Commodity Clusters. Proceedings of the ACM/IEEE Conference on Supercomputing (SC06), Tampa, Florida.

90. **Bergdorf M, Baxter S, Rendlema CA, Shaw DE.** 2016. Desmond/GPU Performance as of November 2016. D E Shaw Research Technical Report DESRES/TR.

Antimicrobial Agents and Chemotherapy
AAC
Antimicrobial Agents and Chemotherapy
Downloaded from http://aac.asm.org/ on April 2, 2020 at GSF/ZENTRALBIBLIOTHEK

Accepted Manuscript Posted Online

91. **Krieger E, Vriend G.** 2014. YASARA View - molecular graphics for all devices - from smartphones to workstations. Bioinformatics **30:**2981-2982.

92. **Sastry GM, Adzhigirey M, Day T, Annabhimoju R, Sherman W.** 2013. Protein and ligand preparation: Parameters, protocols and influence on virtual screening enrichments. J Comput Aid Mol Des **27:**221-234.

93. **Olsson MHM, Sondergaard CR, Rostkowski M, Jensen JH.** 2011. PROPKA3: consistent treatment of internal and surface residues in empirical pKa predictions. Journal of Chemical Theory and Computation **7:**525-537.

94. **Søndergaard CR, Olsson MHM, Rostkowski M, Jensen JH.** 2011. Improved Treatment of Ligands and Coupling Effects in Empirical Calculation and Rationalization of pKa Values. Journal of Chemical Theory and Computation **7:**2284-2295.

95. **Harder E, Damm W, Maple J, Wu C, Reboul M, Xiang JY, Wang L, Lupyan D, Dahlgren MK, Knight JL, Kaus JW, Cerutti DS, Krilov G, Jorgensen WL, Abel R, Friesner RA.** 2016. OPLS3: A Force Field Providing Broad Coverage of Drug-like Small Molecules and Proteins. Journal of Chemical Theory and Computation **12:**281-296.

96. **Jorgensen WL, Chandrasekhar J, Madura JD.** 1983. Comparison of simple potential functions for simulating liquid water. The Journal of Chemical Physics **79:**926-935.

Antimicrobial Agents and Chemotherapy

AAC

Antimicrobial Agents and Chemotherapy

Downloaded from http://aac.asm.org/ on April 2, 2020 at GSF/ZENTRALBIBLIOTHEK

Accepted Manuscript Posted Online

Antimicrobial Agents and Chemotherapy

AAC

Antimicrobial Agents and Chemotherapy

Downloaded from http://aac.asm.org/ on April 2, 2020 at GSF/ZENTRALBIBLIOTHEK

Figures

FIG 1. IMP-13 apo and meropenem-bound structures. (A) Overlay of IMP-13 apo structures, with open (magenta) and closed (violet) loops. Zinc-coordinating residues of the open state are shown as sticks. (B) Zoomed view of A showing coordination of the two Zn(II) ions in the apo structures. (C) IMP-13 meropenem-bound structure, loop in orange, ligand in salmon. (D) The closed loop forms a tunnel in the meropenem-bound structure. Zinc ions are shown as gray spheres and water as red spheres.

FIG 2. 2Fo-Fc maps at a contour level of 1σ for the presented complex crystal structures showing interactions of the antibiotics' carbapenem scaffold (A, C, E, G) and tails (B, D, F, H) with IMP-13. Imipenem (E, F – green) shows three distinct tail conformations – all are depicted. Doripenem (A, B – yellow), ertapenem (C, D – magenta) and meropenem (G, H – salmon) are each seen in one conformation in each chain. Interactions are shown as dashed lines: purple – zinc interactions; yellow – H-bonds and charge-charge interactions; orange – aromatic; green – hydrophobic; pale blue – water network. Zinc ions are shown as gray spheres and water as red spheres.

FIG 3 - Summary of molecular dynamics simulations for apo and carbapenem-bound IMP-13. Structures of the hydrolyzed antibiotics, with numbering used in the simulations, are shown in the left column. Column 1 shows the root mean squared fluctuation (RMSF) of the ligand, fitted on the ligand only and on the protein-ligand complex; column 2 the RMSF of the protein Cα atoms and column 3 the RMSF of the protein sidechains. The L1 loop is marked by orange bars on all graphs. Results are shown for doripenem (A), ertapenem (B), impipenem (C) and meropenem (D). Values for apo Cα and sidechain RMSF are shown for comparison in F. Cα and side-chain RMSF values for the key residue Trp28 are shown for all structures in E.

Accepted Manuscript Posted Online

Antimicrobial Agents and Chemotherapy

AAC

Antimicrobial Agents and Chemotherapy

Downloaded from http://aac.asm.org/ on April 2, 2020 at GSF/ZENTRALBIBLIOTHEK

913 **FIG 4. Chemical shift changes between the apo and ertapenem-bound forms of IMP-13.** (A) ^{1}H,^{15}N
914 backbone amide and tryptophan amide sidechain chemical shift changes between the apo and
915 ertapenem-bound forms of IMP-13, for the spectra shown in Fig. SI7 (individually in Fig. SI8 and SI9),
916 plotted against residue number. A representation of the secondary structure of IMP-13 is shown
917 above the plot with β-sheets represented as blue arrows, loops in yellow and α-helices in orange.
918 The L1 region is indicated by red boxes. (B) Shift changes ($\Delta\delta > 0.1$), identified in A, are shown on
919 the ertapenem-bound crystal structure of IMP-13 (PDB: 6RZS).

920

921 **FIG 5. Heteronuclear NOE data showing fast-timescale motions of apo and ertapenem-bound IMP-**
922 **13.** Heteronuclear NOE data of backbone amides and tryptophan indole NεHε measured at 600 MHz
923 (^{1}H frequency) and 25 °C for both the apo (blue) and ertapenem-bound forms (red). The loop 1
924 region is marked with red rectangles. Residues above 224 are removed from the plot as all show
925 negative heteronuclear NOEs in both the apo and ertapenem-bound forms.

926

927 **FIG 6. Comparison of IMP-13 meropenem-bound structure with previously published metallo-β-**
928 **lactamase structures.** IMP-13 is always depicted with an orange loop and the IMP-13-bound
929 meropenem in salmon. (A) and (C) Two views of IMP-13 overlaid with IMP-1 bound to the
930 mercaptocarboxylate inhibitor (yellow - 1DD6 (57)). (B) and (D) Overlay of IMP-13 with NDM-1 and
931 hydrolyzed meropenem (green – 5N0H (67)). The phenylalanine residue at the tip of the loop is not
932 resolved in the structure, but the backbone is shown in sticks. (E) Overlay of IMP-13 with IMP-1
933 bound to the bisthiazoline inhibitor L-VC26 (cyan - 5EWA (58)). (F) Overlay of IMP-13 with IMP-1
934 bound to a phosphonate-based inhibitor (purple - 5HH4 (61)).

935

Accepted Manuscript Posted Online

936 **FIG 7. Comparison of PBP-3 and IMP-13 binding to meropenem.** View of the carbapenem scaffold in
937 (A) and (C) and of the tail moieties in (B) and (D). Interactions are shown as dashed lines: purple –
938 zinc interactions; yellow – H-bonds and charge-charge interactions; orange – aromatic; green –
939 hydrophobic; pale blue – water network

Antimicrobial Agents and Chemotherapy

AAC

Antimicrobial Agents and Chemotherapy

Downloaded from http://aac.asm.org/ on April 2, 2020 at GSF/ZENTRALBIBLIOTHEK

Accepted Manuscript Posted Online
Antimicrobial Agents and Chemotherapy
AAC
Antimicrobial Agents and Chemotherapy

Downloaded from http://aac.asm.org/ on April 2, 2020 at GSF/ZENTRALBIBLIOTHEK

Accepted Manuscript Posted Online
Antimicrobial Agents and Chemotherapy
AAC
Antimicrobial Agents and Chemotherapy

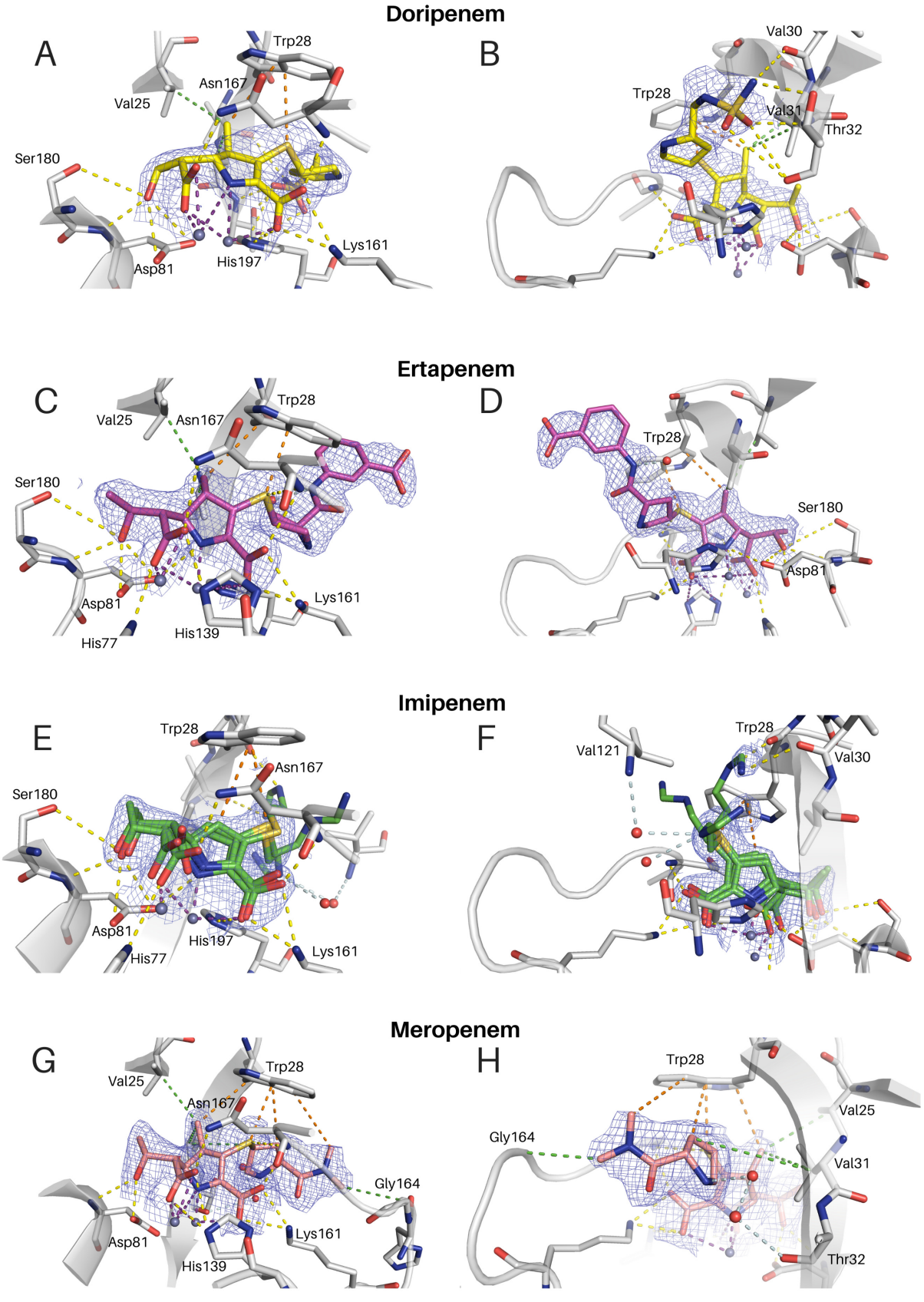

Downloaded from http://aac.asm.org/ on April 2, 2020 at GSF/ZENTRALBIBLIOTHEK

Accepted Manuscript Posted Online
Antimicrobial Agents and Chemotherapy
AAC
Antimicrobial Agents and Chemotherapy

RMSF of ligand, fit on ligand only and protein-ligand complex by atom

RMSF of C-alphas by residue

RMSF of sidechains by residue

A Doripenem:

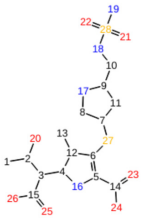

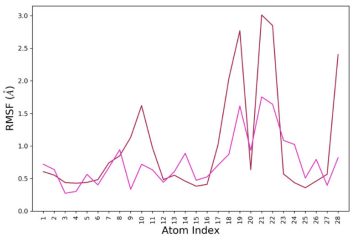

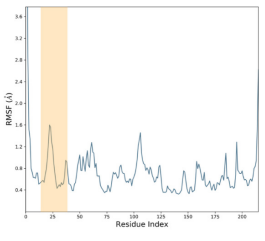

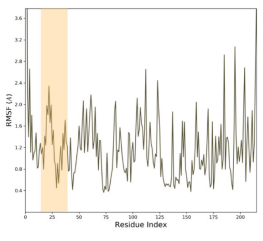

B Ertapenem:

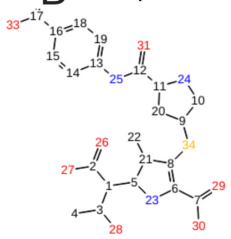

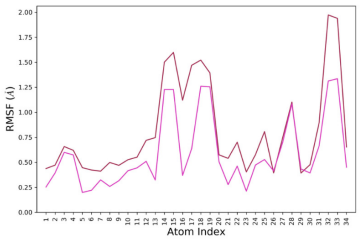

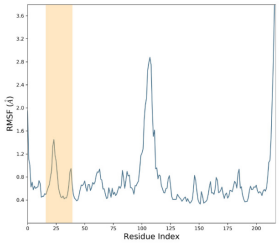

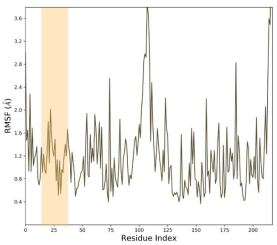

C Imipenem:

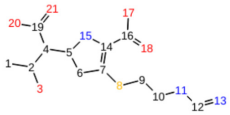

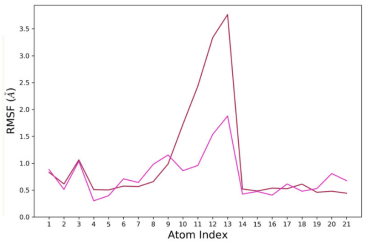

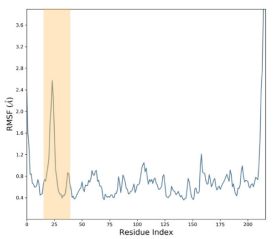

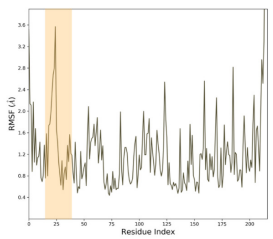

D Meropenem:

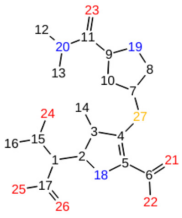

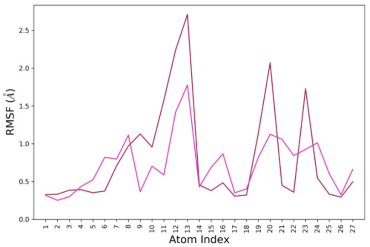

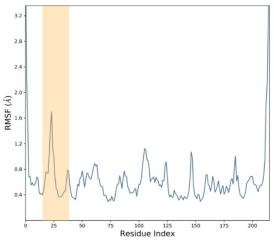

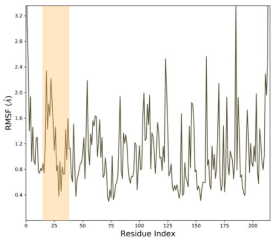

E

Trp28 atom RMSF C-Alpha vs Side Chain

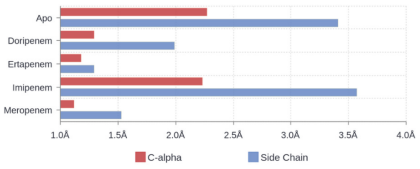

F Apo:

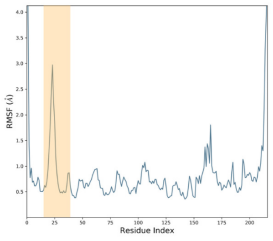

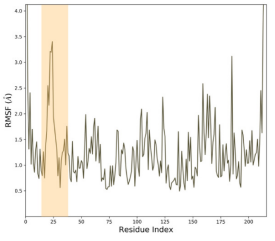

Downloaded from http://aac.asm.org/ on April 2, 2020 at GSF/ZENTRALBIBLIOTHEK

Accepted Manuscript Posted Online

Antimicrobial Agents and Chemotherapy

AAC

Antimicrobial Agents and Chemotherapy

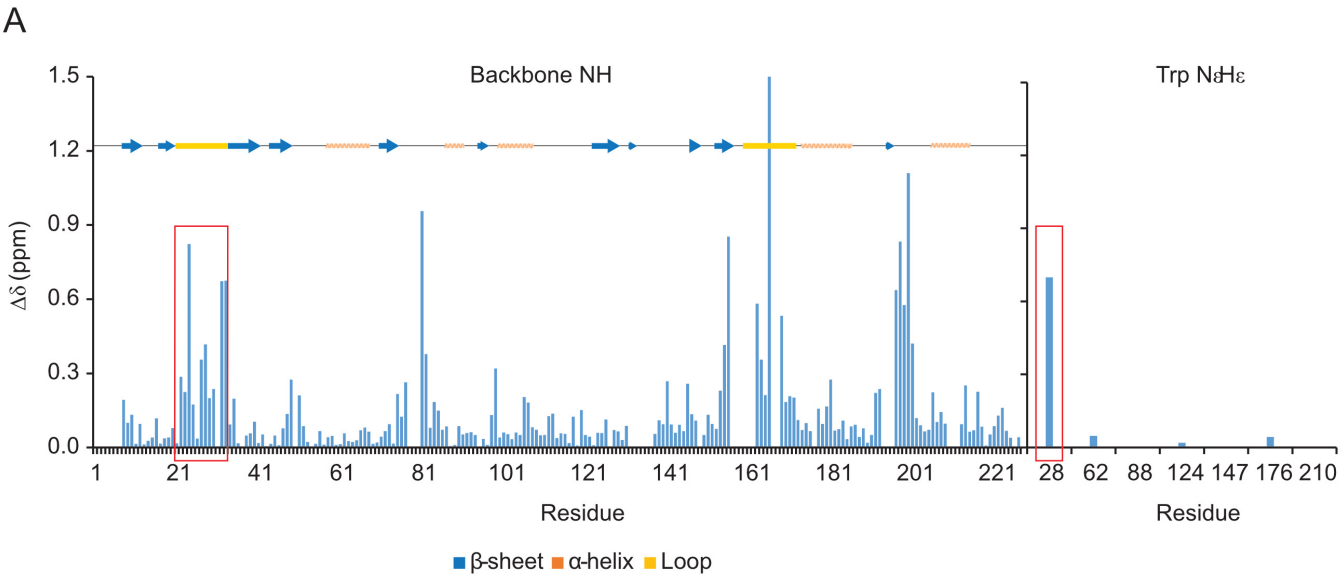

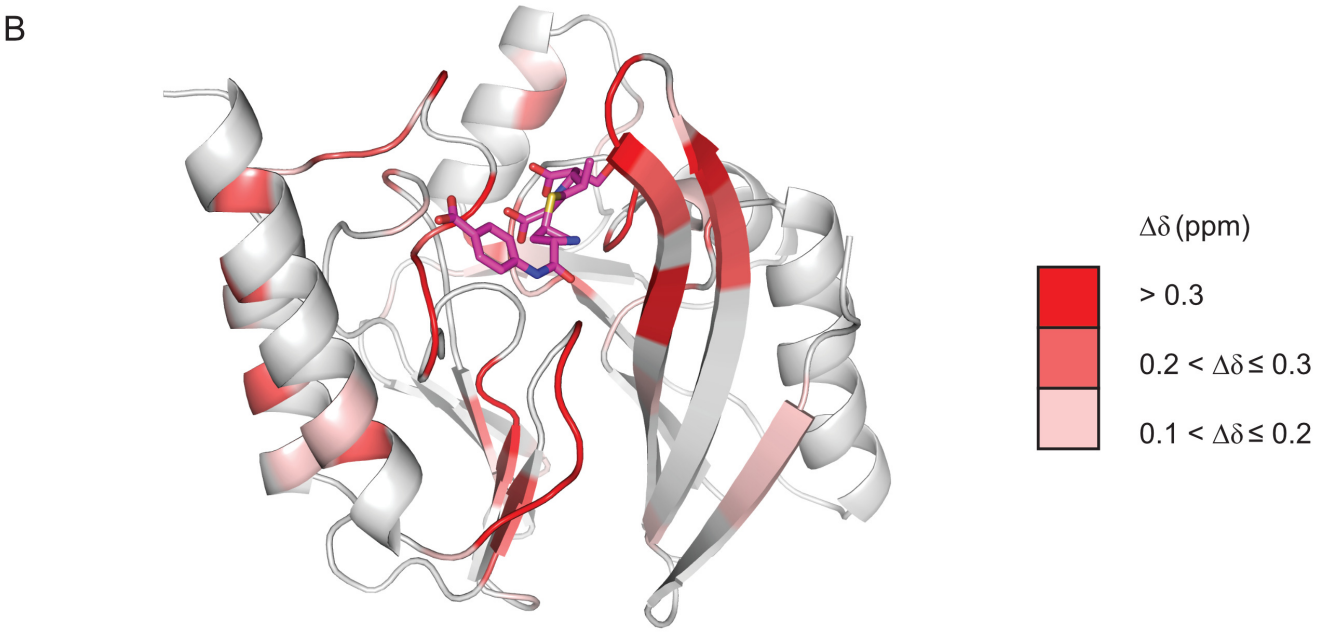

Downloaded from http://aac.asm.org/ on April 2, 2020 at GSF/ZENTRALBIBLIOTHEK

Accepted Manuscript Posted Online

Antimicrobial Agents and Chemotherapy

AAC

Antimicrobial Agents and Chemotherapy

Downloaded from http://aac.asm.org/ on April 2, 2020 at GSF/ZENTRALBIBLIOTHEK

Accepted Manuscript Posted Online
Antimicrobial Agents and Chemotherapy
AAC
Antimicrobial Agents and Chemotherapy

Downloaded from http://aac.asm.org/ on April 2, 2020 at GSF/ZENTRALBIBLIOTHEK

Accepted Manuscript Posted Online

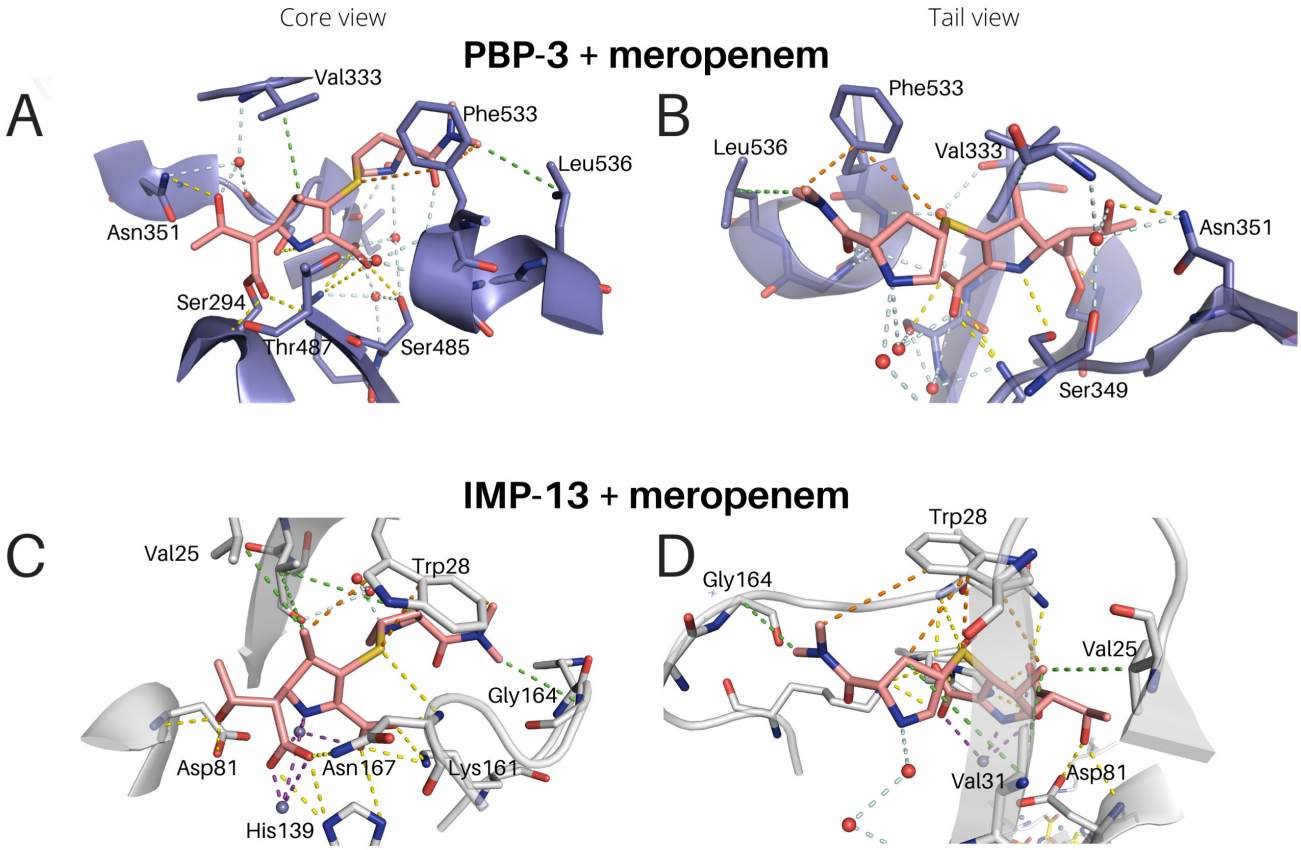

Downloaded from http://aac.asm.org/ on April 2, 2020 at GSF/ZENTRALBIBLIOTHEK

AAC
Antimicrobial Agents and Chemotherapy

Antimicrobial Agents and Chemotherapy